Journal of Computational Physics 231 (2012) 6801–6826

Contents lists available at SciVerse ScienceDirect

Journal of Computational Physics

journal homepage: www.elsevier.com/locate/jcp

A non-negative moment-preserving spatial discretization scheme for the linearized Boltzmann transport equation in 1-D and 2-D Cartesian geometries

Peter G. Maginot, Jim E. Morel *, Jean C. Ragusa

Department of Nuclear Engineering, Texas A&M University, College Station, TX 77843, USA

ARTICLE INFO

Article history:
Received 24 August 2011
Received in revised form 8 March 2012
Accepted 12 June 2012
Available online 26 June 2012

Keywords:
Strictly non-negative closure
Discrete ordinates method
Radiation transport
Discontinuous finite elements

ABSTRACT

We present a new nonlinear spatial finite-element method for the linearized Boltzmann transport equation with S_n angular discretization in 1-D and 2-D Cartesian geometries. This method has two central characteristics. First, it is equivalent to the linear-discontinuous (LD) Galerkin method whenever that method yields a strictly non-negative solution. Second, it always satisfies both the zeroth and first spatial moment equations. Because it yields the LD solution when that solution is non-negative, one might interpret our method as a classical fix-up to the LD scheme. However, fix-up schemes for the LD equations derived in the past have given up solution of the first moment equations when the LD solution is negative in order to satisfy positivity in a simple manner. We present computational results comparing our method in 1-D to the strictly non-negative linear exponential-discontinuous method and to the LD method. We present computational results in 2-D comparing our method to a recently developed LD fix-up scheme and to the LD scheme. It is demonstrated that our method is a valuable alternative to existing methods.

1. Introduction

The linearized Boltzmann transport equation describes the transport of radiation or particles that interact with a background medium but have no self interactions. Examples of such particles include neutrons and gamma rays. The S_n or discrete-ordinates method is perhaps the most popular and widely used angular discretization for this equation. Spatial discretization methods for the S_n equations can produce negative angular flux solutions, which are clearly non-physical. Such negativities can arise in 1-D Cartesian geometry calculations only in optically thick cells but, in multidimensional Cartesian geometries, negativities can also arise in voids. Characteristic methods based upon polynomial scattering source representations of degree greater than zero, such as the Linear Characteristic method (LC) are always non-negative in 1-D geometry as long as the projected scattering source remains non-negative. In 2-D such methods are always positive as long as the projected scattering source and projected outflow boundary fluxes remain positive [1]. The Step Characteristic method (SC), which is based upon a constant scattering source representation [1], is strictly positive and formally second-order accurate, but it can be particularly inaccurate in multidimensional calculations due to a high degree of numerical diffusion resulting from the constant dependence of the angular flux that is assumed on cell faces. Furthermore, unlike most higher-order characteristic methods, the step method possesses neither the intermediate [2] nor the thick diffusion limit [3,4]. This can make it require an over-resolved mesh for even mildly diffusive problems.

* Corresponding author.
E-mail addresses: pmaginot@tamu.edu (P.G. Maginot), morel@tamu.edu (J.E. Morel), jean.ragusa@tamu.edu (J.C. Ragusa).

0021-9991/$ - see front matter © 2012 Elsevier Inc. All rights reserved.
http://dx.doi.org/10.1016/j.jcp.2012.06.018

Several methods to eliminate or mitigate negativities have been devised in the past. Such methods can generally be divided into two categories: (1) so-called ad-hoc "fix-ups" and (2) inherently non-negative nonlinear moments methods. An example of the former type is the diamond difference scheme with set-to-zero fix-up [5], while examples of the latter include various exponential characteristic methods [6–8].

Ad-hoc fix-up schemes have been traditionally related to moments methods with non-smooth closures. Hence, their associated equations have generally been solved via a fixed-point iteration rather than Newton's method. This fixed-point approach is always effective for purely absorbing problems, but when scattering is present, it has been found to interact poorly with sophisticated convergence acceleration schemes such as the diffusion-synthetic acceleration (DSA) method [9], particularly in problems where acceleration is most needed [10]. If acceleration techniques are not applied, the fixed-point approach is generally effective, but unacceptably slow convergence is obtained in highly diffusive problems.

Inherently non-negative nonlinear methods, such as the linear exponential characteristic method and the linear exponential discontinuous finite-element method (ED) [11], have smooth nonlinearities and thus can be solved using Newton's method. However, characteristic methods are expensive, particularly on non-orthogonal meshes, and cannot be applied in curvilinear coordinates. Although exponential finite-element methods are less complicated than characteristic methods and can be applied in curvilinear coordinates (assuming an exponential representation in angle as well as in space), they can suffer from a lack of fine-mesh accuracy relative to analogous polynomial-based discontinuous finite-element schemes. For instance, Wareing showed that, in 1-D slab-geometry, ED can be less accurate than the linear-discontinuous Galerkin finite-element method (LD) when the mesh is highly refined [11].

Our purpose here is to devise a new nonlinear spatial finite-element method for the S_n equations in 1-D and 2-D Cartesian geometries. This method has two central characteristics. First, it is equivalent to the LD scheme whenever LD yields a strictly non-negative solution. Second, the new scheme always satisfies both the zeroth and first spatial moment equations. Because it yields the LD solution when that solution is non-negative, one could interpret our method as a fix-up scheme. However, fix-up schemes defined in the past for the LD equations do not satisfy the first moment equation when the LD solution is negative in order to satisfy positivity in a simple manner [12].

The equations associated with our scheme are not smooth, but they are everywhere continuous and the Jacobian matrix is discontinuous at only a finite number of points. Since our equations do not have a continuous Jacobian, the applicability of Newton's method might seem to be questionable. However, Fichtl, et al., [13] have recently been able to reliably apply Newton's method to the LD equations using a traditional fix-up scheme having a continuous set of equations with a pointwise-discontinuous Jacobian.

Work for this paper originally began as the 2-D extension of another strictly non-negative finite-element closure for the zeroth and first S_n moment equations [14]. However, some practical implementation difficulties together with the results of Fichtl, et al., motivated us to develop the present approach, yielding an inherently non-negative finite-element scheme. The new method presented herein represents the discontinuous finite-element analog of a characteristic scheme originally developed for both slab and rectangular geometries by Mathews and Minor [15,16]. Qualitatively, the new method assumes an angular flux distribution within a cell that is defined to be equal to a linear function at all points for which that linear function is non-negative, and zero at all points for which that linear function is negative. Given a valid set of spatial moments, an angular flux representation having those moments can be uniquely constructed using this formulation. While we have not formally proved this property, we have successfully tested it numerically. In particular, we have been able to specify a valid set of moments and then solve for the corresponding representation having those moments. The only caveat is that the method becomes increasingly ill-conditioned as the specified moments approach those of a delta-function at either of the cell endpoints. This same type of ill-conditioning occurs with the exponential discontinuous representation, and can be expected to occur with essentially any representation that does not explicitly contain delta-functions. Since our general angular flux representation is obtained from a linear function via a set-to-zero procedure, we refer to our new technique as the consistent set-to-zero method (CSZ).

The linear S_n equations are generally solved via source iteration [5]. Each source iteration requires the inversion of an independent block lower-triangular system for each direction and energy in a process known as a sweep. Since our equations are nonlinear, we use Newton's method to solve our equations. There are two ways to implement this method. The first is to apply Newton's method to each independent set of sweep equations, effectively solving a nonlinear system for each scattering source iterate. In this case, Newton's method is nested within the source iteration process. An important property of this approach is that the independent nonlinear sweep equations for each direction and energy can be solved one spatial cell at a time. Hence the nonlinear systems that must be individually solved are quite small. In addition, storing the full angular flux iterate can be avoided simply by re-starting the nonlinear iterations with a zero guess for each source iteration. More specifically, once the angular flux solution for a single cell, direction, and energy is obtained and the associated contributions to both the scattering source in that cell and the inflow source for the next downstream cell are computed, the angular flux solution for that cell, direction, and energy can be discarded. The ability to avoid storage of the full angular flux iterate is the primary advantage of this approach. This approach has traditionally been used to solve nonlinear S_n equations. For many years after the introduction of S_n codes, storage of the full angular flux solution was simply not practical, and it is still often avoided today. The primary disadvantage of this approach is that if one is to apply convergence acceleration techniques to the source iteration process, they must be applied to a nonlinear system. DSA has been applied to nonlinear forms of the transport equation [17], but nonlinear DSA is far less theoretically understood and potentially much less robust than linear DSA.

The second implementation approach is to apply Newton's method to the full system of equations as opposed to the sweep equations. In this case, the source iteration process is nested within the Newton iteration process. The primary disadvantage of this approach is that one must store the full angular flux iterate across Newton iterations. However, the primary advantage of this approach is that it is compatible with standard linear convergence acceleration schemes. For instance, DSA can applied to the Jacobian equation, which is linear. Fichtl, et al., [13] used this second approach, solving the Jacobian equations with a sweep-preconditioned Krylov method, but they did not attempt to apply DSA or any other acceleration technique.

We have chosen to implement the Newton iterations within the source iterations since this represents the simplest approach and enables us to test the accuracy and efficiency of our method relative to existing schemes, which we solve in the same manner. Applying acceleration to our nonlinear equations remains a current research topic and represents a significant complication that is beyond the scope of this paper.

The remainder of this paper is organized as follows: the derivation for the CSZ method is presented first for slab geometry (Section 2) and then for 2-D Cartesian geometry (Section 3). The solution techniques used to solve the resulting equations are discussed in Section 4. Numerical results are provided for slab geometry in (Section 5.1) and for 2-D Cartesian geometry (Section 5.2). Conclusions and recommendations for future work are given in Section 6.

2. Slab geometry derivation

The S_n transport equation in 1-D Cartesian geometry is

$$\mu_d \frac{d\psi}{dx} + \sigma_t \psi(x,\mu_d) = S(x,\mu_d), \quad d = 1, N_d, \tag{1}$$

where μ_d is the d'th direction cosine that defines the particle direction with respect to the x-axis, ψ is the angular flux (particles/cm^2 s sr) at position x in direction μ_d, σ_t is the total macroscopic cross section (cm^{-1}), and S is the total source (scattering plus inhomogeneous) (particles/cm^3 s sr). The number of directions, N_d for an S_n approximation is equal to n. For the case of isotropic scattering,

$$S(x,\mu_d) = \frac{1}{4\pi}\sigma_s(x)\phi(x) + q(x,\mu_d), \tag{2}$$

where σ_s is the macroscopic scattering cross section (cm^{-1}), q is the inhomogeneous source (particles/cm^3 s sr) in μ_d, and ϕ is the scalar flux (particles/cm^3 s) analytically given by

$$\phi(x) = 2\pi \int_{-1}^{+1} \psi(x,\mu)\, d\mu \tag{3}$$

and calculated via quadrature:

$$\phi(x) = \sum_{d=1}^{N_d} \psi(x,\mu_d) w_d, \tag{4}$$

where w_d is the weight associated with direction μ_d. Note that Eqs. (3) and (4) imply that the weights sum to 4π.

To define a spatial discretization for Eq. (1), we need only consider a single arbitrary mesh cell. This is true in 1-D geometries as well as in multidimensional geometries. The global system of equations is easily obtained from the equations for a single cell by equating the outflow angular fluxes from each cell with the inflow angular fluxes in adjacent cells.

Consider an arbitrary spatial mesh cell with index i, defined for all $x \in [x_{i-1/2,}, x_{i+1/2}]$. We denote the width of the cell by Δx_i, where $\Delta x_i = x_{i+1/2} - x_{i-1/2}$. For simplicity, we elect to use a generic reference element defined for $s \in [0,1]$. This linear transformation reference to physical coordinates is:

$$x = x_{i-1/2} + s\Delta x_i, \tag{5}$$

where it is easy to confirm that when $s = 0$, $x = x_{i-1/2}$ and when $s = 1$, $x = x_{i+1/2}$. The zeroth and first spatial moments of Eq. (1) over cell i are obtained by successively multiplying that equation with basis functions $P_0(s) = 1$ and $P_1(s) = 2s - 1$, and integrating the resultant equations over the cell to respectively get (after algebraic manipulation):

$$\frac{\mu_d}{\Delta x_i}\left(\psi_{i+1/2,d} - \psi_{i-1/2,d}\right) + \sigma_{t,i,d}\psi_{A,i,d} = S_{A,i,d} \tag{6a}$$

and

$$\frac{3\mu_d}{\Delta x_i}\left(\psi_{i+1/2,d} - \psi_{i-1/2,d} - 2\psi_{A,i,d}\right) + \sigma_{t,i,d}\psi_{X,i,d} = S_{X,i,d}, \tag{6b}$$

where $\sigma_{t,i}$ is the total cross section of cell i, $\psi_{i-1/2,d} = \psi(0,\mu_d)$, and $\psi_{i+1/2,d} = \psi_d(1,\mu_d)$. The average and slope quantities, $\psi_{A,i,d}$ and $\psi_{X,i,d}$, are defined using our local coordinate system as:

$$\psi_{A,i,d} = \int_0^1 P_0(s)\psi(s,\mu_d)ds, \tag{7a}$$

$$\psi_{X,i,d} = 3\int_0^1 P_1(s)\psi(s,\mu_d)ds. \tag{7b}$$

Eqs. (6a) and (6b) have three unknowns, $\psi_{A,i,d}$, $\psi_{X,i,d}$, and the cell outflow, $\psi_{i\pm1/2,d}$, depending on the sign of μ_d. The inflow is known either from boundary conditions or from the solution in the adjacent upstream cell. For brevity, we limit our discussion to positive μ_d, so $\psi_{i+1/2,d}$ is the cell outflow and $\psi_{i-1/2,d}$ is the known cell inflow. The equations for μ_d negative are easily obtained by analogy. To solve the moment equations and close the system of two equations with three unknowns, a distribution for the angular flux, $\widetilde{\psi}(s)$, within the cell must be assumed. In the following sections, we derive various schemes based on the choice of $\widetilde{\psi}(s)$.

2.1. LD derivation

The LD scheme assumes a linear angular flux distribution within each cell:

$$\widetilde{\psi}_{LD}(s) = a_{LD}P_0(s) + b_{LD}P_1(s). \tag{8}$$

Calculating $\psi_{A,i,d}, \psi_{X,i,d}$, and $\psi_{i+1/2,d}$ using Eq. (8), we obtain the following LD relationships for the cell unknowns:

$$\psi_{A,i,d} = a_{LD}, \tag{9a}$$

$$\psi_{X,i,d} = b_{LD}, \tag{9b}$$

$$\psi_{i+1/2,d} = a_{LD} + b_{LD}. \tag{9c}$$

Substituting the definitions of Eqs. (9) into Eqs. (6) creates a system of two linear equations entirely defined in terms of a_{LD} and b_{LD}, which then completely defines $\widetilde{\psi}(s)_{LD}$ within cell i. Further, since the 2×2 system is linear, one can solve for a_{LD} and b_{LD} in terms of $\psi_{A,i,d}$ and $\psi_{X,i,d}$ and make $\psi_{A,i,d}$ and $\psi_{X,i,d}$ the primary unknowns.

2.2. ED derivation

For the exponential discontinuous scheme, the formulation of the $\widetilde{\psi}(s)$ basis function can take on several different forms; however all forms must be equivalent to an exponential with a linear argument. In Wareing's development of the ED method [11], the flux distribution $\widetilde{\psi}$ was represented as:

$$\widetilde{\psi}(s) = c_1 e^{c_2 P_1(s)}. \tag{10}$$

In our replication of ED (for comparison purposes), we formulate $\widetilde{\psi}$ slightly differently. To ensure that $\widetilde{\psi}$ remains non-negative at all times during the iteration process, the parameter, c_1, was moved into the exponential term:

$$\widetilde{\psi}_{ED}(s) = e^{c_1 P_0(s) + c_2 P_1(s)}. \tag{11}$$

Hereafter, ED will be synonymous with the formulation described by Eq. (11). The reader is directed to [11] for a more complete derivation of the ED method including consideration of multidimensional Cartesian geometries. The definitions of $\psi_{A,i,d}$, $\psi_{X,i,d}$, and $\psi_{i+1/2,d}$ for the exponential method described by Eq. (11) are given below:

$$\psi_{A,i,d} = \frac{e^{c_1}}{2c_2}(e^{c_2} - e^{-c_2}), \tag{12a}$$

$$\psi_{X,i,d} = \frac{3}{2c_2^2}((c_2-1)e^{c_1+c_2} + (c_2+1)e^{c_1-c_2}), \tag{12b}$$

$$\psi_{i+1/2,d} = e^{c_1+c_2}. \tag{12c}$$

Unlike LD, the relationships in Eqs. (12) are nonlinear and cannot be directly inverted to express c_1 and c_2 in terms of $\psi_{A,i,d}$ and $\psi_{X,i,d}$. Thus, c_1 and c_2 remain the primary unknowns, requiring a nonlinear search to find the parameters c_1 and c_2 that indirectly define $\psi_{A,i,d}, \psi_{X,i,d}$, and $\psi_{i+1/2,d}$. As in the case of LD, substituting the definitions of Eqs. (12) into Eqs. (6) creates a system of two equations defined entirely in terms of only two unknowns, c_1 and c_2, which then fully define $\widetilde{\psi}_{ED}(s)$. However, unlike LD, this system of equations is nonlinear. Discussions pertaining to the solution techniques employed are provided in Section 4.1.

2.3. CSZ derivation

We now define our consistent set-to-zero scheme, which is a strictly non-negative modification of the LD scheme. One of the primary objectives of the CSZ scheme is to yield the LD solution whenever that solution is everywhere non-negative within the cell. This is achieved by using the LD angular flux representation if it is everywhere non-negative within the cell,

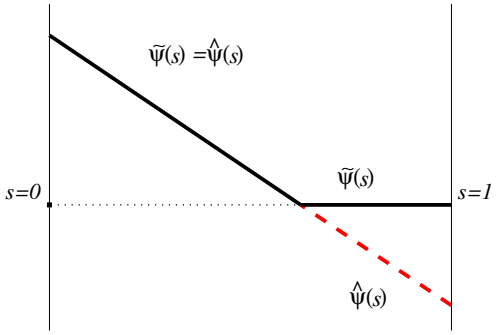

Fig. 1. Graphical definition of $\widetilde{\psi}_{csz}(s)$.

and otherwise using a representation that is a combination of a constant zero dependence and a linear dependence. Specifically,

$$\widetilde{\psi}_{csz}(s) = \begin{cases} \hat{\psi}_{csz}(s) & \text{if } \hat{\psi}_{csz}(s) \geqslant 0, \\ 0 & \text{otherwise}, \end{cases} \tag{13}$$

where

$$\hat{\psi}_{csz}(s) = a_{csz}P_0(s) + b_{csz}P_1(s). \tag{13a}$$

This representation is illustrated in Fig. 1. Note that this definition leads to a continuous but not differentiable transition between the LD and non-LD representations used in the CSZ scheme. In slab geometry, the behavior of $\widetilde{\psi}_{csz}(s)$ in cell i is characterized by one of the following three cases:

1. non-negative everywhere (LD definitions apply – see Eqs. (9)), or,
2. non-negative for $s < s_z$ only, or,
3. non-negative for $s > s_z$ only,

where s_z is the value of s at which $\hat{\psi}_{csz}(s_z) = 0$:

$$s_z = \frac{1}{2}\left(1 - \frac{a_{csz}}{b_{csz}}\right). \tag{14}$$

Cases 2 and 3 apply only when s_z lies within the cell. The parameters a_{csz} and b_{csz} are clearly equal to their LD counterparts a_{LD} and b_{LD} when $\hat{\psi}_{csz}(s)$ is strictly non-negative within the cell. For cases 2 and 3, $\widetilde{\psi}_{csz}(s)$ is 0 over a portion of the cell, so the spatial integrations in Eqs. (7a) and (7b) can be restricted to that portion of the cell for which $\widetilde{\psi}_{csz} > 0$. For case 2, we simply substitute from Eq. (13a) into Eqs. (7a) and (7b) and integrate over the interval $[0, s_z]$:

$$\psi_{A,i,d} = s_z(a_{csz} + b_{csz}(s_z - 1)), \tag{15a}$$

$$\psi_{X,i,d} = s_z\left(4b_{csz}s_z^2 + 3(b_{csz}(1 - 2s_z) + a_{csz}(s_z - 1))\right). \tag{15b}$$

For case 3, we substitute Eq. (13a) into Eqs. (7a) and (7b) but integrate over the interval $[s_z, 1]$:

$$\psi_{A,i,d} = (1 - s_z)(a_{csz} + b_{csz}s_z), \tag{15c}$$

$$\psi_{X,i,d} = (1 - s_z)(b_{csz} + s_z(3a_{csz} - 2b_{csz}(1 - 2s_z))). \tag{15d}$$

In slab geometry the cell outflow, $\psi_{i+1/2,d}$, is simply equal to $\widetilde{\psi}(1)$. Applying Eq. (13), we have:

$$\psi_{i+1/2,d} = \begin{cases} a_{csz} + b_{csz} & \text{if } \hat{\psi}_{csz}(1) \geqslant 0, \\ 0 & \text{otherwise}. \end{cases} \tag{16}$$

We have now defined expressions for $\psi_{A,i,d}$, $\psi_{X,i,d}$, and $\psi_{i+1/2,d}$ in terms of the two unknowns a_{csz} and b_{csz}, making Eqs. (6) a closed nonlinear system of equations for a_{csz} and b_{csz}.

3. 2-D rectangular geometry derivation

In rectangular geometry, the S_n transport equation becomes:

$$\mu_d \frac{\partial \psi}{\partial x} + \eta_d \frac{\partial \psi}{\partial y} + \sigma_t \psi = S, \quad d = 1, N_d, \tag{17}$$

where η_d is the direction cosine with respect to the y-axis, both ψ and S are functions of the variables $x,\ y,\ \eta_d$, and μ_d, and S is the total source that includes both scattering and inhomogeneous contributions. Eqs. (2) and (4) still apply, but in 2-D for a standard "triangular" quadrature set, $N_d = n(n+2)/2$.

We begin our derivation by first considering an arbitrary spatial mesh cell with index $i,\ j$, defined for all $x \in [x_{i-1/2}, x_{i+1/2}]$ and $y \in [y_{j-1/2}, y_{j+1/2}]$. We denote the widths of the cell as $\Delta x_i = x_{i+1/2} - x_{i-1/2}$ and $\Delta y_j = y_{j+1/2} - y_{j-1/2}$. Again, we transform to a generic reference cell:

$$x = x_{i-1/2} + s\Delta x_i, \tag{18}$$
$$y = y_{j-1/2} + t\Delta y_j. \tag{19}$$

Cell edges are denoted as shown in Fig. 2. The zeroth and first spatial moments of Eq. (17) over cell $i,\ j$ are obtained by successively multiplying that equation with basis functions $P_0(s,t) = 1$, $P_{1S}(s,t) = 2s - 1$, and $P_{1T}(s,t) = 2t - 1$, and integrating the resultant equations over the cell to respectively yield:

$$\frac{\mu_d}{\Delta x_i}\left(\psi_{i+1/2,j,d} - \psi_{i-1/2,j,d}\right) + \frac{\eta_d}{\Delta y_j}\left(\psi_{i,j+1/2,d} - \psi_{i,j-1/2,d}\right) + \sigma_{t,i,j}\psi_{A,i,j,d} = S_{A,i,j,d}, \tag{20a}$$
$$\frac{3\mu_d}{\Delta x_i}\left(\psi_{i+1/2,j,d} + \psi_{i-1/2,j,d} - 2\psi_{A,i,j,d}\right) + \frac{\eta_d}{\Delta y_j}\left(\psi_{M,i,j+1/2,d} - \psi_{M,i,j-1/2,d}\right) + \sigma_{t,i,j}\psi_{X,i,j,d} = S_{X,i,j,d}, \tag{20b}$$
$$\frac{\mu_d}{\Delta x_i}\left(\psi_{M,i+1/2,j,d} - \psi_{M,i-1/2,j,d}\right) + \frac{3\eta_d}{\Delta y_j}\left(\psi_{i,j+1/2,d} + \psi_{i,j-1/2,d} - 2\psi_{A,i,j,d}\right) + \sigma_{t,i,j}\psi_{Y,i,j,d} = S_{Y,i,j,d}. \tag{20c}$$

Eqs. (20) apply to all directions, but for conciseness and without loss of generality, we limit our treatment to $\mu_d > 0$ and $\eta_d > 0$. The other three cases are easily obtained by analogy. For $\mu_d > 0$ and $\eta_d > 0$, the known inflow quantities are $\psi_{i,j-1/2,d}, \psi_{i-1/2,j,d}, \psi_{M,i,j-1/2,d}$, and $\psi_{M,i-1/2,j,d}$, and the unknown outflow quantities are $\psi_{i,j+1/2,d}$, $\psi_{i+1/2,j,d}$, $\psi_{M,i,j+1/2,d}$, and $\psi_{M,i+1/2,j,d}$. The edge unknowns are defined as:

$$\psi_{i+1/2,j,d} = \int_0^1 \psi_d(1,t)dt, \tag{21a}$$
$$\psi_{i,j+1/2,d} = \int_0^1 \psi_d(s,1)ds, \tag{21b}$$
$$\psi_{M,i+1/2,j,d} = 3\int_0^1 P_{1T}(1,t)\psi_d(1,t)dt, \tag{21c}$$
$$\psi_{M,i,j+1/2,d} = 3\int_0^1 P_{1S}(s,1)\psi_d(s,1)ds. \tag{21d}$$

The unknown cell integral quantities of Eqs. (20), $\psi_{A,i,j,d}$, $\psi_{X,i,j,d}$, and $\psi_{Y,i,j,d}$, are defined regardless of streaming direction as follows:

$$\psi_{A,i,j,d} = \int_0^1\int_0^1 P_0(s,t)\psi_d(s,t)dsdt, \tag{22a}$$
$$\psi_{X,i,j,d} = 3\int_0^1\int_0^1 P_{1S}(s,t)\psi_d(s,t)dsdt, \tag{22b}$$
$$\psi_{Y,i,j,d} = 3\int_0^1\int_0^1 P_{1T}(s,t)\psi_d(s,t)dsdt. \tag{22c}$$

As in slab geometry, the moment equations, Eqs. (20), have more unknowns than equations and thus require the assumption of an angular flux representation, $\tilde{\psi}(s,t)$, in order to close the system of equations.

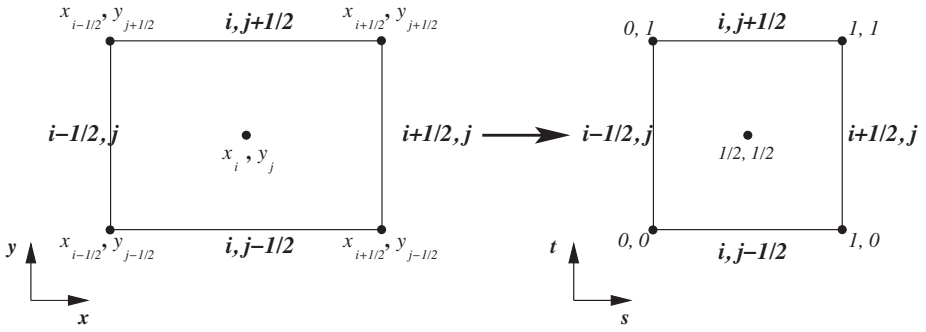

Fig. 2. Graphical explanation of the nomenclature associated with cell $i,\ j$.

3.1. LD derivation

In 2-D Cartesian geometry, the LD scheme assumes an angular flux distribution that is linear in s and t:

$$\widetilde{\psi}_{LD}(s,t) = a_{LD}P_0(s,t) + b_{LD}P_{1S}(s,t) + c_{LD}P_{1T}(s,t). \tag{23}$$

Applying the definitions of Eqs. (21) and Eqs. (22) yield the following relations for the unknowns of Eqs. (20), defined entirely in terms of 3 unknowns, $a_{LD},\ b_{LD}$, and c_{LD}:

$$\psi_{i,j+1/2,d} = a_{LD} + c_{LD}, \tag{24a}$$
$$\psi_{i+1/2,j,d} = a_{LD} + b_{LD}, \tag{24b}$$
$$\psi_{M,i+1/2,j,d} = c_{LD}, \tag{24c}$$
$$\psi_{M,i,j+1/2,d} = b_{LD} \tag{24d}$$

and

$$\psi_{A,i,j,d} = a_{LD}, \tag{25a}$$
$$\psi_{X,i,j,d} = b_{LD}, \tag{25b}$$
$$\psi_{Y,i,j,d} = c_{LD}. \tag{25c}$$

Substituting Eqs. (24) and (25) into Eqs. (20) (the moment equations) yields a 3×3 linear system of equations defined entirely in terms of $a_{LD},\ b_{LD}$, and c_{LD}, which in turn defines $\widetilde{\psi}_{LD}(s,t)$.

3.2. CSZ derivation

We now extend the CSZ scheme to 2-D Cartesian geometries. The basic principle of the closure remains the same as in 1-D. A primary objective of the CSZ scheme is to yield the LD solution whenever that solution is everywhere non-negative within the cell. As in 1-D, this is achieved by using the LD angular flux representation if it is everywhere non-negative within the cell, and otherwise using a representation that is a combination of a constant zero solution and a linear dependence. In particular,

$$\widetilde{\psi}_{csz}(s,t) = \begin{cases} \hat{\psi}_{csz}(s,t) & \text{if } \hat{\psi}_{csz}(s,t) \geqslant 0, \\ 0 & \text{otherwise}, \end{cases} \tag{26}$$

where

$$\hat{\psi}_{csz}(s,t) = a_{csz}P_0(s,t) + b_{csz}P_{1S}(s,t) + c_{csz}P_{1T}(s,t). \tag{26a}$$

3.2.1. CSZ edge derivation

We next relate the edge unknowns defined by Eqs. (21) to the coefficients associated with Eqs. (26). We first consider edge $i,\ j+1/2$. The dependence of $\widetilde{\psi}_{csz}$ along this edge is characterized by one of the following 4 cases:

1. everywhere non-negative (in which case the LD outflow definitions of Eq. (24) apply), or,
2. non-negative for $s < s_z$ only, or,
3. non-negative $s > s_z$ only, or,
4. everywhere 0,

where s_z is the point at which $\hat{\psi}_{csz}(s_z,1) = 0$:

$$s_z = \frac{1}{2}\left(1 - \frac{a_{csz} + c_{csz}}{b_{csz}}\right). \tag{27}$$

Cases 2 and 3 apply only when s_z lies on edge $i,\ j+1/2$. The integrations for case 1 have previously been given (see the preceding Section 3.1), and the integrations for case 4 are trivial. The edge quantities of rectangular geometry are very similar to the cell quantities of slab geometry Eqs. (15a) and (15b). The integrals defined in Eqs. (21b) and (21d) can be limited to the non-zero portion of edge $i,\ j+1/2$. For case 2, we need only integrate over $s \in [0, s_z]$, yielding the following results:

$$\psi_{i,j+1/2,d} = s_z(a_{csz} + c_{csz} + b_{csz}(s_z - 1)), \tag{28}$$

$$\psi_{M,i,j+1/2,d} = s_z\left[4b_{csz}s_z^2 + 3(b_{csz} - a_{csz} - c_{csz}) + 3s_z(a_{csz} - 2b_{csz} + c_{csz})\right]. \tag{29}$$

For case 3 we need only integrate over $s \in [s_z, 1]$, yielding:

$$\psi_{i,j+1/2,d} = -(s_z - 1)(a_{csz} + c_{csz} + b_{csz}s_z), \tag{30}$$

$$\psi_{M,i,j+1/2,d} = -(s_z - 1)(b_{csz}(1 + 2s_z(2s_z - 1)) + 3s_z(a_{csz} + c_{csz})). \tag{31}$$

The CSZ definitions for the unknowns along edge $i + 1/2,\ j$ are analogous to those along edge $i,\ j + 1/2$. Again, the dependence of $\widetilde{\psi}_{csz}$ is characterized by one of the following 4 cases:

1. everywhere non-negative (in which case the LD outflow definitions of Eqs. (24) apply), or,
2. non-negative for $t < t_z$ only, or,
3. non-negative $t > t_z$ only, or,
4. everywhere 0,

where t_z is the point at which $\hat{\psi}_{csz}(1,t) = 0$:

$$t_z = \frac{1}{2}\left(1 - \frac{a_{csz} + b_{csz}}{c_{csz}}\right). \tag{32}$$

Cases 2 and 3 apply only if t_z lies on edge $i + 1/2,\ j$. Again, the integrations for case 1 have been previously given, and the integrations for case 4 are trivial. For case 2 along edge $i + 1/2,\ j$ we have:

$$\psi_{i+1/2,j,d} = t_z(a_{csz} + b_{csz} - c_{csz}(t_z - 1)), \tag{33}$$

$$\psi_{M,i+1/2,j,d} = t_z\left(3(c_{csz} - b_{csz} - a_{csz}) + 3t_z(a_{csz} + b_{csz} - 2c_{csz}) + 4c_{csz}t_z^2\right). \tag{34}$$

For case 3 along edge $i + 1/2,\ j$ we have:

$$\psi_{i+1/2,j,d} = -(t_z - 1)(a_{csz} + b_{csz} + c_{csz}t_z), \tag{35}$$

$$\psi_{M,i+1/2,j,d} = -(t_z - 1)(c_{csz} + t_z(3(a_{csz} + b_{csz}) - 2c_{csz}(1 - 2t_z))). \tag{36}$$

3.3. CSZ cell derivation

We next relate the interior moments, $\psi_{A,i,j,d},\ \psi_{X,i,j,d}$, and $\psi_{Y,i,j,d}$, to the coefficients of the angular flux representation defined in Eqs. (26). We first note that the behavior of $\widetilde{\psi}_{csz}$ within cell $i,\ j$ is characterized by one of the 5 following cases:

1. $\widetilde{\psi}_{csz}$ is everywhere non-negative (LD definitions apply; see Eq. (25)), or,
2. $\widetilde{\psi}_{csz} > 0$ at only 3 of 4 corners, or,
3. $\widetilde{\psi}_{csz} > 0$ at only 2 of 4 corners, or,
4. $\widetilde{\psi}_{csz} > 0$ at only 1 of 4 corners, or,
5. $\widetilde{\psi}_{csz}$ is everywhere 0.

Fig. 3 illustrates the above cases. The integrations have been previously given for case 1 and are trivial for case 5. However, integration for cases 2-4 is not a simple task as it requires the use of variable limits of integration. We have chosen to decompose the cell into triangles to perform the integrals. More specifically, for cases 2-4 the non-zero portions of the cell are decomposed into N_T triangular areas as shown in Fig. 4. Let $\mathbf{T_k}$ denote the k'th such triangle. The flux moments defined in Eq. (22) can be expressed in terms of integrals over each triangle as follows:

$$\psi_{A,i,j,d} = \sum_{k=1}^{N_T} \int\int_{\mathbf{T_k}} P_0(s,t)\hat{\psi}_{csz}(s,t)\,ds\,dt, \tag{37}$$

$$\psi_{X,i,j,d} = \sum_{k=1}^{N_T} 3 \int\int_{\mathbf{T_k}} P_{1S}(s,t)\hat{\psi}_{csz}(s,t)\,ds\,dt, \tag{38}$$

$$\psi_{Y,i,j,d} = \sum_{k=1}^{N_T} 3 \int\int_{\mathbf{T_k}} P_{1T}(s,t)\hat{\psi}_{csz}(s,t)\,ds\,dt. \tag{39}$$

These integrals are carried out via Barycentric integration.[18] The Barycentric coordinates, λ_1 and λ_2, are mapped to the physical coordinates, s and t, as follows:

$$s = \lambda_1 s_1 + \lambda_2 s_2 + (1 - \lambda_1 - \lambda_2)s_3, \tag{40a}$$

$$t = \lambda_1 t_1 + \lambda_2 t_2 + (1 - \lambda_1 - \lambda_2)t_3. \tag{40b}$$

where A_k is the area of $\mathbf{T_k}$, and $\{s_i, t_i\}_{i=1}^3$, are its vertices as shown in Fig. 5. Using the Barycentric coordinates, each integral takes the following general form:

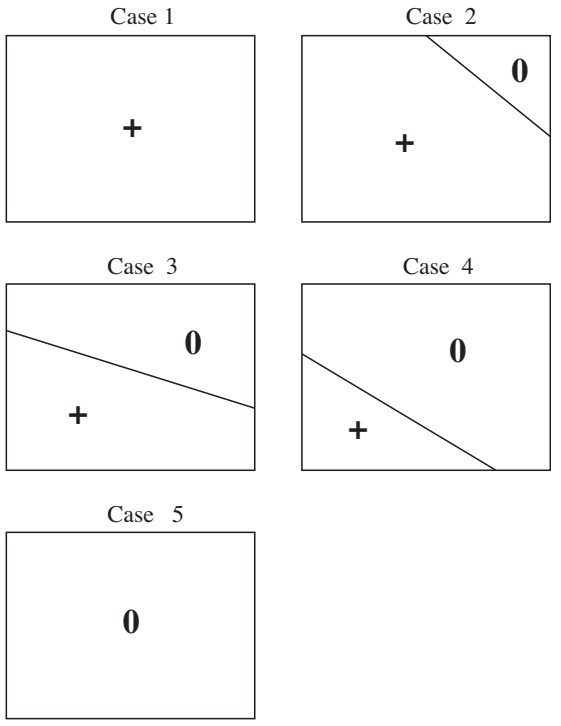

Fig. 3. All possible forms of the interior cell shape $\widetilde{\psi}(s,t)$ in the CSZ method.

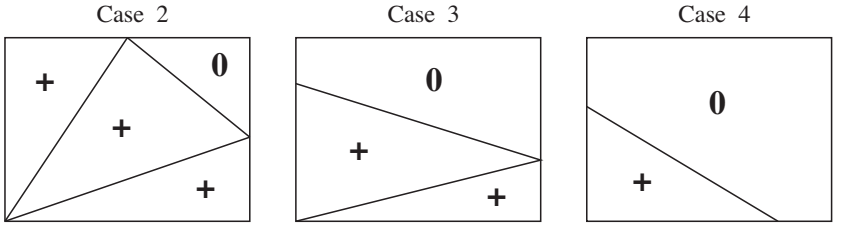

Fig. 4. Triangular decomposition of $\widetilde{\psi}_{CSZ}(s,t)$ in cell i, j.

$$\int_{\mathbf{T_k}} f(\mathbf{r})dr = 2A_k \int_0^1 \int_0^{1-\lambda_2} f(\lambda_1\mathbf{v_1} + \lambda_2\mathbf{v_2} + (1-\lambda_1-\lambda_2\mathbf{v_3})d\lambda_1 d\lambda_2, \tag{41}$$

where $\mathbf{v_i} = (s_i, t_i)^T$. More specifically:

$$\int\int_{\mathbf{T_k}} P_0(s,t)\hat{\psi}_{csz}(s,t)dsdt = A_k\left(a_{csz} - b_{csz} - c_{csz} + \frac{2b_{csz}}{3}(s_1+s_2+s_3) + \frac{2c_{csz}}{3}(t_1+t_2+t_3)\right), \tag{42}$$

$$\begin{aligned} 3\int\int_{\mathbf{T_k}} P_{1S}(s,t)\hat{\psi}_{csz}(s,t)dsdt &= A_k(3(b_{csz} - a_{csz} + c_{csz}) + (2a_{csz} - 4b_{csz} - 2c_{csz})(s_1+s_2+s_3) - 2c_{csz}(t_1+t_2+t_3) \\ &+2b_{csz}(s_1^2+s_2^2+s_3^2) + 2b_{csz}(s_1s_2+s_1s_3+s_2s_3) + c_{csz}s_1(2t_1+t_2+t_3) + c_{csz}s_2(t_1+2t_2+t_3) + c_{csz}s_3(t_1+t_2+2t_3)) \end{aligned} \tag{43}$$

and

$$\begin{aligned} 3\int\int_{\mathbf{T_k}} P_{1T}(s,t)\hat{\psi}_{csz}dsdt &= A_k(3(b_{csz} - a_{csz} + c_{csz}) + (2a_{csz} - 2b_{csz} - 4c_{csz})(t_1+t_2+t_3) - 2b_{csz}(s1+s2+s3) \\ &+2c_{csz}(t_1^2+t_2^2+t_3^2) + b_{csz}s_1(2t_1+t_2+t_3) + b_{csz}s_2(t_1+2t_2+t_3) + b_{csz}s_3(t_1+t_2+2t_3) + 2c_{csz}(t_1t_2+t_1t_3+t_2t_3), \end{aligned} \tag{44}$$

where Eqs. (42)–(44) are used to compute the components of $\psi_{A,i,j,d}$, $\psi_{X,i,j,d}$, and $\psi_{Y,i,j,d}$, respectively, from triangle $\mathbf{T_k}$. All Barycentric integrations were performed using the symbolic manipulation package in MATLAB [19].

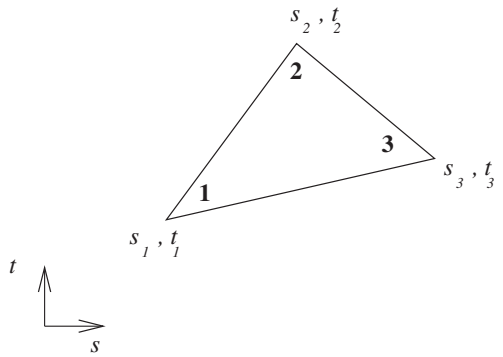

Fig. 5. Explanation of the coordinates of triangle $\mathbf{T_k}$.

Using the previously described integration techniques, all of the unknowns in the moment equations can be defined entirely in terms of the unknowns, a_{csz}, b_{csz}, and c_{csz}. Substituting these relationships into Eqs. (20) creates a closed 3×3 nonlinear system of equations for the three unknowns, a_{csz}, b_{csz}, and c_{csz}.

3.4. Strictly non-negative comparator for CSZ in rectangular geometry

The ED scheme was used in slab geometry to compare CSZ to a strictly non-negative solution representation that preserves the moment equations. The relative traits of the ED scheme compared to LD and CSZ are not expected to change in the move from slab to rectangular geometry. As such, it is more beneficial to compare CSZ to a different method of obtaining a strictly non-negative angular flux solution, an ad-hoc fix-up, in rectangular geometry. We compare CSZ to a rectangular $x - y$ ad-hoc fix-up we developed based on a scheme presented by Hamilton, Benzi, and Warsa [20] for a triangular mesh. We refer to our rectangular analog of their scheme as the Warsa-like (WL) scheme. It is a nonlinear scheme based on the LD scheme that generates angular flux solutions with strictly non-negative outflows. Like CSZ, WL is meant to yield the LD solution when the LD solution is considered acceptable. The properties of the WL scheme are as follows:

1. WL guarantees only non-negative angular flux *outflows*,
2. WL does not conserve the full set of moment equations if LD yields a negative outflow,
3. WL *does* conserve particle balance.

The WL scheme assumes a linear angular flux representation within a cell:

$$\widetilde{\psi}_{WL}(s,t) = a_{WL}P_0(s,t) + b_{WL}P_{1S}(s,t) + c_{WL}P_{1T}(s,t). \tag{45}$$

Since WL and LD use identical linear representations for $\widetilde{\psi}(s,t)$, we first introduce notation to refer to the value of $\widetilde{\psi}(s,t)$ for a given method at an outflow vertex of cell i, j. Vertices 1, 2, and 3 have s and t coordinates of $(0,1),(1,1)$, and $(1,0)$, respectively, as shown in Fig. 2. $\psi_{k,m}$ is the value of $\widetilde{\psi}(s,t)$ at an outflow vertex k for method m, where $m = LD$ or WL. For $\mu_d > 0$ and $\eta_d > 0$, $\psi_{k,m}$ are defined as follows:

$$\psi_{1,m} = a_m - b_m + c_m, \tag{46a}$$
$$\psi_{2,m} = a_m + b_m + c_m, \tag{46b}$$
$$\psi_{3,m} = a_m + b_m - c_m. \tag{46c}$$

The equations used to find a_{WL}, b_{WL}, and c_{WL} depend on the number of negative $\psi_{k,LD}$:

1. all $\psi_{k,LD} > 0$ or,
2. one $\psi_{k,LD} < 0$ or,
3. two $\psi_{k,LD} < 0$ or,
4. three $\psi_{k,LD} < 0$.

If all $\psi_{k,LD} > 0$, then $\widetilde{\psi}_{WL} = \widetilde{\psi}_{LD}$ and no further work is required. However, if any $\psi_{k,LD} < 0$ (cases 2–4), Eqs. (20) do not yield a linear representation of $\widetilde{\psi}(s,t)$ that is everywhere non-negative along the cell outflows. Thus, a new system of equations is required to find suitable coefficients a_{WL}, b_{WL}, and c_{WL} that will yield a strictly non-negative linear representation of $\widetilde{\psi}_{WL}$ along the outflow edges of cell i, j. Without loss of generality, we consider case 2 and let the negative $\psi_{k,LD}$ be $\psi_{1,LD}$ (i.e, the LD representation yields a negative angular flux for vertex 1). Based on [20], the new system of equations consists of:

1. the balance equation, Eq. (20a),
2. an explicit statement that $\psi_{1,WL} = 0$,

$$a_{WL} - b_{WL} + c_{WL} = 0,$$

3. a scaling of non-negative outflows, $\frac{\psi_{2,LD}}{\psi_{3,LD}} = \frac{\psi_{2,WL}}{\psi_{3,WL}}$,

$$\frac{\psi_{2,LD}}{\psi_{3,LD}} = \frac{a_{WL} + b_{WL} + c_{WL}}{a_{WL} + b_{WL} - c_{WL}}.$$

For case 3, let us assume that $\psi_{1,LD}$ and $\psi_{2,LD}$ are negative. Again, drawing from Warsa's previous work for triangular meshes, the WL equations consist of

1. the balance equation, Eq. (20a),
2. an explicit statement that $\psi_{1,WL} = 0$:

$$a_{WL} - b_{WL} + c_{WL} = 0,$$

3. an explicit statement that $\psi_{2,WL} = 0$:

$$a_{WL} + b_{WL} + c_{WL} = 0.$$

There is no direct parallel between the rectangular mesh case 4 and the triangular mesh scheme presented in [20] since there are two outflow vertices at most in a triangular mesh, as opposed to at most three in a rectangular mesh. Since there are only three unknowns, a_{WL}, b_{WL}, and c_{WL}, Setting the solution to zero at three vertices completely defines the solution, leaving the balance equation unsatisfied. This is clearly undesirable. Fortunately, we have not observed three negative outflow values in the problems we considered. That is not to say that it cannot happen, but rather that it did not occur in our testing.

Since both WL and LD always produce solutions with a linear dependence within a cell, the relationships between the vertex values of $\widetilde{\psi}_{WL}$ and the linear expansion coefficients a_{WL}, b_{WL}, and c_{WL} are completely analogous to those for LD:

$$\psi_{i,j+1/2,d} = a_{WL} + c_{WL}, \tag{47a}$$
$$\psi_{i+1/2,j,d} = a_{WL} + b_{WL}, \tag{47b}$$
$$\psi_{M,i+1/2,j,d} = c_{WL}, \tag{47c}$$
$$\psi_{M,i,j+1/2,d} = b_{WL} \tag{47d}$$

and

$$\psi_{A,i,j,d} = a_{WL}, \tag{48a}$$
$$\psi_{X,i,j,d} = b_{WL}, \tag{48b}$$
$$\psi_{Y,i,j,d} = c_{WL}. \tag{48c}$$

We stress that while the LD, ED, and CSZ methods always satisfy the zeroth and first moment equations, the WL method only satisfies all of these moment equations in some cases. In other cases, only the zeroth moment equation is satisfied in conjunction with auxiliary equations that assure positivity.

4. Solution techniques and computational metrics

In this section we present the solution techniques, error measures, reference solutions, and measures of computational effort used to generate our computational results.

4.1. Solution techniques

4.1.1. Linear source iteration

The linear Boltzmann equation describing the transport of particles is written as:

$$\mathbf{L}\Psi = \mathbf{S}\Psi + \mathbf{q}, \tag{49}$$

with $\mathbf{L}$, the streaming plus interaction operator, $\mathbf{S}$, the scattering operator, $\mathbf{q}$, the external source term, and ψ the angular flux. In slab geometry.

$$\mathbf{L}\psi = \mu\frac{\partial\psi}{\partial x} + \sigma_t(x)\psi(x,\mu), \tag{50}$$

$$\mathbf{S}\psi = \sum_{\ell=0}^{L}\frac{(2\ell+1)}{4\pi}\sigma_{s,\ell}(x)\phi_\ell(x)P_\ell(\mu), \tag{51}$$

where L is the order of the scattering source expansion, ϕ_ℓ is the ℓth angular moment of the angular flux:

$$\phi_\ell(x) = \sum_{d=1}^{N_{dir}} w_d\psi_d(x)P_\ell(\mu_d), \tag{52}$$

$\sigma_{s,\ell}$ is the ℓth order scattering cross section, $P_\ell(\mu_d)$ is the ℓth Legendre polynomial in μ_d, and N_{dir} is the number of discrete ordinates directions considered. Analogs of the above equations in 2-D Cartesian geometry are omitted here for brevity but without loss of generality because Eq. (49) applies in all geometries. It is important to note that since for many cases $L \ll N_{dir} - 1$, the $\mathbf{S}$ operator is of relatively low angular rank. Typically, this is taken advantage of by storing only the moments of the angular flux vector, ϕ_ℓ, and not the full ψ vector.

Note that all angular coupling occurs on the right side of Eq. (49) through the scattering source term. Thus the left side of Eq. (49) consists of independent advection-reaction equations for each direction. This suggests the standard S_n solution technique for solving Eq. (49) whereby the scattering source term is lagged:

$$\mathbf{L}\psi^{\ell+1} = \mathbf{S}\psi^{\ell} + \mathbf{q} = \mathbf{Q}^{\ell}. \tag{53}$$

For obvious reasons, this is called source iteration. When standard spatial discretizations are applied, the algebraic structure of each advection-reaction equation is block lower-diagonal, with each block corresponding to the angular flux unknowns for a given direction in a given spatial cell. Thus $\mathbf{L}$ can be inverted one angular direction at a time, and for each direction, the spatial solution can be sequentially carried out one cell at a time starting at the entrant boundary where the incident flux is known from boundary conditions and proceeding in the direction of flow. This approach is typically referred to as a transport sweep. An exception occurs with a reflective boundary condition when the entrant flux is a function of the exiting flux rather than explicitly specified. In this case, the boundary coupling is then lagged along with the scattering source.

4.1.2. Nonlinear source iteration

All of the nonlinear methods we have considered, ED, CSZ, and WL, are solved using a nonlinear form of source iteration previously discussed in Section (1). We have opted to solve the transport equation using a nonlinear form of source iteration in which Newton iteration is nested within source iteration. Specifically, the nonlinear sweep equations for each scattering source iterate are solved using Newton's method. This is particularly simple since this requires independent 2×2 (1-D) or 3×3 (2-D) systems to be solved for each direction in each cell as the sweep progresses. Furthermore, because the independent systems being solved are so small, acceptable efficiency can be achieved by starting the Newton iteration anew with each souce iteration, thereby avoiding the need to store the angular flux vector. Rather, one need only store the low-rank vector of Legendre flux moments associated with the scattering source. We have opted to use this approach in order to avoid the memory expense. Finally, we stress that this is the approach that has been traditionally used to solve the transport equation with nonlinear spatial discretizations.

4.1.3. Commonalities of SI for all methods considered

Convergence of the source iteration process was based on the normalized change in the cell average scalar flux, $\Delta\phi_{A,i,l}$:

$$\Delta\phi_{A,i}^{\ell} = \frac{|\phi_{A,i}^{\ell} - \phi_{A,i}^{\ell-1}|}{|\phi_{A,i}^{\ell}|}, \tag{54}$$

where i is the cell index and ℓ is the number of source iterations completed. Iteration was stopped on the condition that:

$$\max_{1\leqslant i\leqslant N_{cells}}\left[\frac{|\phi_{A,i}^{\ell} - \phi_{A,i}^{\ell-1}|}{|\phi_{A,i}^{\ell}|}\right] \leqslant 10^{-6}, \tag{55}$$

where N_{cells} is the total number of cells in the problem.

4.1.4. Solving for $\widetilde{\psi}$-LD specific

The LD equations are strictly linear, and are solved using the source iteration process that has been previously discussed. In 1-D each source iteration is performed by the direct solution of a 2×2 matrix system for each direction and spatial cell. In 2-D each source iteration requires the direct solution of a 3×3 matrix system for each direction and spatial cell.

4.1.5. Solving for $\widetilde{\psi}$-ED specific

The initial guess for parameters c_1 and c_2 is found by linearly expanding the definitions of Eqs. (12a)–(12c) about an arbitrary pair of iterates, c_{1*} and c_{2*}, and taking the limit as $c_{2*} \to 0$. This yields the following definitions:

$$\psi_{i+1/2} = e^{c_{1*}} + (c_1 - c_{1*})e^{c_{1*}} + c_2 e^{c_{1*}}, \tag{56a}$$

$$\psi_A = e^{c_{1*}} + (c_1 - c_{1*})e^{c_{1*}}, \tag{56b}$$

$$\psi_X = c_2 e^{c_{1*}}. \tag{56c}$$

Inserting Eqs. (56) directly into Eqs. (6) yields a linear system of equations in terms of unknowns c_1 and c_2. Note that Eqs. (56) are equivalent to the LD equations, so the LD solution is the initial guess for the ED method. After the first guess is computed, c_1 and c_2 are obtained using Newton's method and an analytically formed Jacobian. We stress that the Newton iterations are nested within the source iterations and that the Newton iterations are restarted each source iteration to reduce storage requirements. Thus an initial guess is computed at the start of each source iteration.

4.1.6. Solving for $\widetilde{\psi}$- CSZ specific

The initial guess for CSZ is the LD solution, $\widetilde{\psi}_{LD} = \hat{\psi}_{CSZ}$. If $\hat{\psi}_{CSZ} \geqslant 0$ everywhere within a cell, $\widetilde{\psi}_{LD} = \widetilde{\psi}_{csz}$. Otherwise, the nonlinear CSZ definitions for the unknowns of Eqs. (6) or Eqs. (20) are applied, and Newton's method with an analytical Jacobian is used to solve the nonlinear system of equations. CSZ has an everywhere defined Jacobian, but the Jacobian is discontinuous at a finite number of points. Nonetheless, Newton iteration worked in all of our test problems. Similar results for equations with a discontinuous Jacobian were observed by Ficthl, et. al [13]. As in the case of ED, the Newton iterations are nested within the source iterations.

4.1.7. Solving for $\widetilde{\psi}$- ED and CSZ commonalities

The nonlinear iteration used to solve the ED and CSZ equations is of the form:

$$f^{n+1} = f^n + \alpha \Delta f^n,$$

where f is the vector of coefficients, e.g. $[c_1, c_2]^T$ or $[a_{csz}, b_{csz}, c_{csz}]^T$, n is the nonlinear iteration index, and α is a step-length damping parameter. Standard Newton iteration corresponds to $\alpha = 1$. However, if the Newton search for the ED or CSZ parameters that describe $\widetilde{\psi}$ does not find a solution rapidly, indicating that Newton's method may be diverging, the iteration is reset to the initial guess, and a damped value of $0 < \alpha \leqslant 1$ is used. Though not the most advanced technique, this method always converged in our test problems to the correct global solution. More sophisticated nonlinear search techniques, such as step length selection based on a given iterate's minimization of the residual formed by the moment equations, as suggested in [21] were attempted. However, it was observed that these techniques quite frequently found localized, but not the global minimum of the moment equations, effectively failing to find a solution. Thus, the more sophisticated techniques were abandoned, and the crude, but effective, step length adjustment based on iteration duration was used.

To assure uniform levels of convergence, the CSZ and ED nonlinear iteration convergence is based on the normalized change of $\psi_{A,i,d}$ in slab geometry and $\psi_{A,i,j,d}$ in rectangular geometry between Newton iterations n and $n-1$. For slab and rectangular geometries respectively:

$$\frac{|\psi^n_{A,i,d} - \psi^{n-1}_{A,i,d}|}{|\psi^n_{A,i,d}|} \leqslant 10^{-8}, \tag{57a}$$

$$\frac{|\psi^n_{A,i,j,d} - \psi^{n-1}_{A,i,j,d}|}{|\psi^n_{A,i,j,d}|} \leqslant 10^{-8}. \tag{57b}$$

4.1.8. Solving for $\widetilde{\psi}$- WL specific

The WL scheme begins by first finding $\widetilde{\psi}_{LD}$ and checking the calculated outflow for positivity. If $\widetilde{\psi}_{LD}$ is non-negative along the entire outflow of cell i,j, then $\widetilde{\psi}_{LD} = \widetilde{\psi}_{WL}$. Otherwise, a second matrix inversion is required to solve the WL linear equations (*not* the moment equations) appropriate to correcting the number of negative vertices associated with $\widetilde{\psi}_{LD}$. After the 2nd matrix inversion, the WL scheme is complete; WL requires at most two iterations to find a_{WL}, b_{WL}, and c_{WL}.

4.2. Error measures

We measure error by the L_2 norm between the numerically calculated scalar flux average, $\phi_{A,num,i}$, and the reference solution, $\phi_{A,ref,i}$:

$$Error = \sqrt{\sum_{i=1}^{N_{cells}} \left[V_i \left(\phi_{A,ref,i} - \phi_{A,num,i} \right)^2 \right]}, \tag{58}$$

where V_i refers to the volume of cell i, and N_{cells} is the total number of cells in the problem. In 1-D geometry, $V_i = \Delta x_i$ and in 2-D $V_i = \Delta x_i \Delta y_j$. $\phi_{A,num,i}$ is calculated as follows:

$$\phi_{A,num,i} = \sum_{d=1}^{N_{dir}} w_d \psi_{A,i,d}. \tag{59}$$

The method used to calculate $\phi_{A,ref,i}$ in each test problem is discussed in the following sections.

4.3. Reference solution calculation

4.3.1. Slab geometry- $\phi_{A,ref,i}$ in a pure absorber

For the case of a homogeneous pure absorber (Section 5.1.2) with macroscopic absorption cross section σ_a, and flux $\psi_{0,d}$ entrant only at the left boundary (centered at $x = 0$), the exact S_n scalar flux solution, $\phi_{A,ref,i}$ may be calculated as:

$$\phi_{A,ref,i} = \sum_{d=1}^{N_{dir}} \left[\frac{1}{\Delta x_i} \int_{x_{i-1/2}}^{x_{i+1/2}} \left[w_d \psi_{0,d} e^{-\sigma_a x/\mu_d} dx \right] \right]. \tag{60}$$

4.3.2. Slab geometry- $\phi_{A,ref,i}$ in a scattering medium

To calculate $\phi_{A,ref,i}$ in slab geometry for more general problems, i.e. those with scattering and fixed sources (Sections 5.1.3 and 5.1.4) the analytic scalar flux solution provided in [22] was used. The reference average flux $\phi_{A,ref,i}$ was calculated not by exact integration, as in Eq. (60), but rather by using 2 point Gauss integration.

4.3.3. Rectangular geometry- $\psi_{A,ref,i}$ in a void

In the case of a voided medium with a beam of radiation incident along the bottom face of the medium in the direction μ_d and $\eta_d = \sqrt{1-\mu_d^2}$ with vacuum boundary conditions along all other faces, and no fixed sources, the analytic solution for $\psi_{A,ref,i}$ is straightforward to calculate as it is the fraction of cell i, j that lies below the line $y = \frac{\eta_d}{\mu_d} x$.

4.3.4. Rectangular geometry- $\phi_{A,ref,i}$ for variations on the standard iron water problem

Due to the complexity of our variation of the standard iron-water problem, an analytic reference solution is not tractable. Instead, a very fine mesh numerical solution was used as the reference solution. The reference solution was obtained from a calculation with a 6400×6400 cell mesh using the LD spatial discretization. Errors of coarse mesh numerical solutions were calculated using the collapsed fine mesh solution as $\phi_{A,ref,i}$.

4.4. Measuring computational effort

4.4.1. Estimating relative computational cost

To measure the relative computational costs of each method, we considered the number of matrix inversions required to solve a problem. As LD is computationally the simplest and cheapest method, we normalize the total number of matrix inversions required by ED, CSZ, and WL to the total required by LD using the same iterative convergence criterion for all the methods. It must be emphasized LD, ED, CSZ, and WL do not necessarily use the same number of source iterations to converge a problem.

LD requires a single matrix inversion for each direction, in every cell, for each source iteration. For ED and CSZ, the number of matrix inversions is equal to the cumulative total of initial LD solutions plus the number of Newton iterations required for every cell and every direction, until the scattering source is converged. WL requires at most two matrix inversions for each cell, direction, and source iteration. Admittedly, there is a nontrivial amount of computational work in addition to matrix inversions required to perform a Newton iteration for the ED and CSZ methods. However, the work measure that we have defined is reasonably accurate, and prefereable to a direct measure of CPU time, which can be difficult in certain computer systems and can depend strongly upon optimal coding for each method.

4.4.2. Estimating efficiency

For our variation of the iron-water problem, we attempt to quantify the computational work of the numerical schemes by computing the relative efficiency of each scheme. We define a quantitative measure of efficiency as:

$$\text{Efficiency} = \frac{1}{\text{Error} \times \text{Work}}, \tag{61}$$

where work is defined as the number of matrix inversions as described in Section 4.4.1, and error is the L_2 difference between a numerical solution at a given coarse resolution and a very fine mesh solution that has been collapsed to the coarse mesh, as described previously.

5. Computational results

5.1. Slab results

5.1.1. Comparison of theoretical outflow and slope values

The fundamental differences between the LD, ED, and CSZ schemes are best illustrated by comparing the normalized outflow values calculated by each method as a function of the normalized slope. Fig. 6 shows the normalized outflow for LD, CSZ, and ED for $\mu > 0$. The normalized slope has a limited domain: $\psi_{X,i,d}/\psi_{A,i,d} \in [-3, +3]$. However, the plot is restricted to $\psi_{X,i,d}/\psi_{A,i,d} \in [-2, +2.5]$ because both the CSZ and ED normalized outflow values increase without bound as the normalized

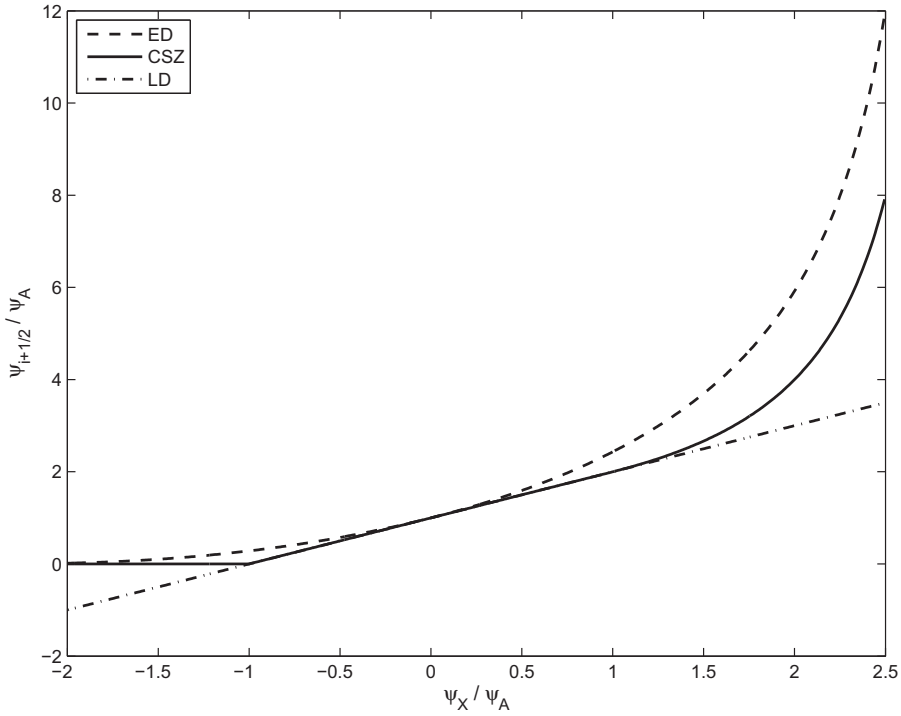

Fig. 6. Slab geometry comparison of LD, ED, and CSZ outflows for $\mu_d > 0$.

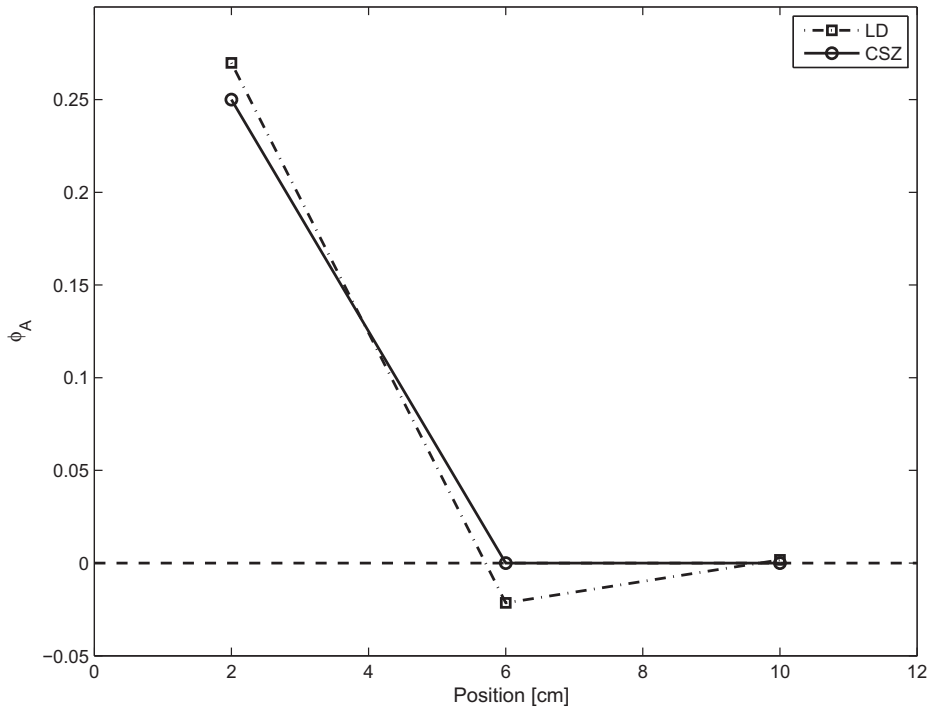

Fig. 7. Average scalar flux comparison of LD and CSZ for a strong absorber with thick cells.

slope value approaches 3 and LD maintains a linear dependence over the entire domain. The outflow plot of Fig. 6 demonstrates several key points:

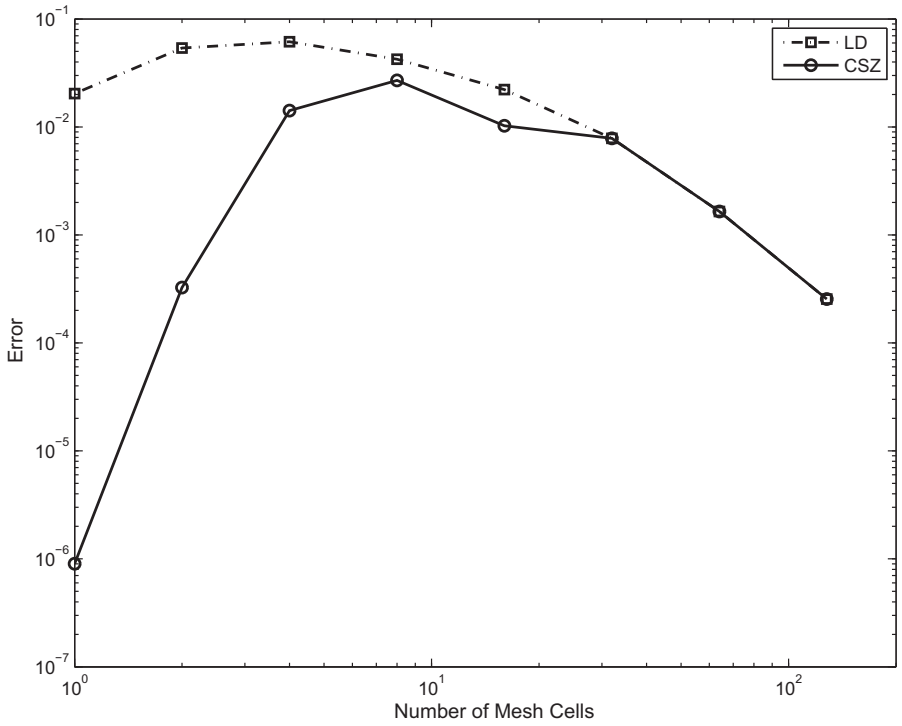

Fig. 8. LD and CSZ rate of convergence plot for the case of a pure absorber.

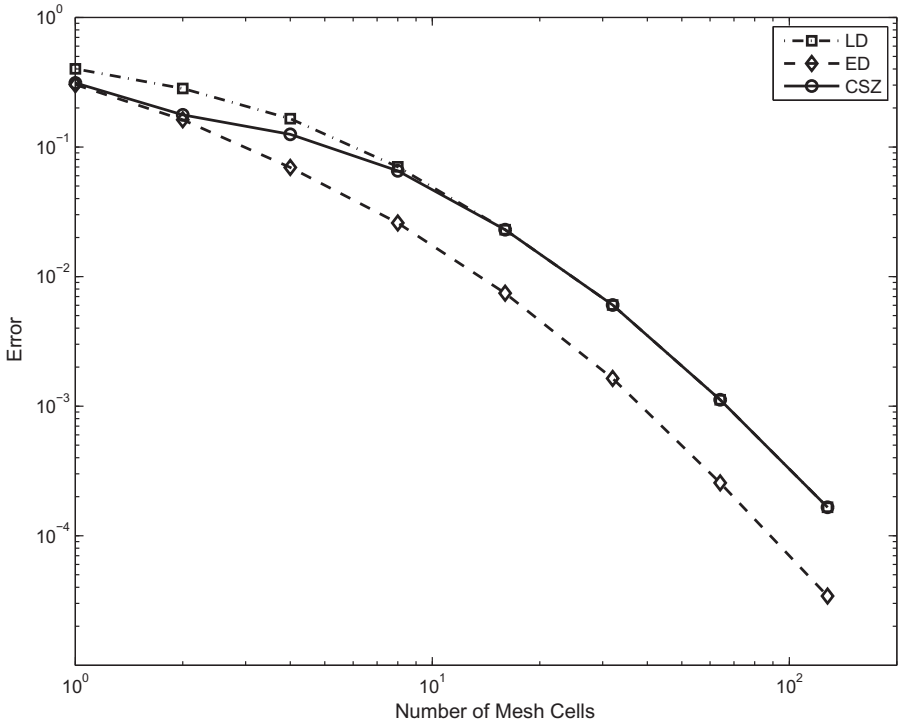

Fig. 9. Rate of convergence for a slab with isotropic incident flux and c = 0.5.

1. both ED and CSZ are strictly non-negative, and LD can yield negative outflows values,
2. both ED and CSZ follow the limit:

$$\lim_{\frac{\psi_{X,i,d}}{\psi_{A,i,d}}\to+3}\left[\frac{\psi_{i+1/2,d}}{\psi_{A,i,d}}\right]=\infty, \tag{62}$$

3. both ED and CSZ follow the limit:

$$\lim_{\frac{\psi_{X,i,d}}{\psi_{A,i,d}}\to-3}\left[\frac{\psi_{i+1/2,d}}{\psi_{A,i,d}}\right]=0, \tag{63}$$

4. CSZ yields the LD solution exactly when the LD solution is everywhere non-negative within the cell ($-1\leqslant\psi_{X,i,d}/\psi_{A,i,d}\leqslant+1$),
5. CSZ is *always* closer to the LD solution than ED is.

5.1.2. Case of a pure absorber

We present now an illustration of the strictly non-negative nature of the new CSZ method as compared to the negativities associated with LD in optically thick cells in slab geometry. Fig. 7 shows the results of a pure absorber problem, with a total slab width of 12 cm, $\sigma_t=\sigma_a=1$ cm^{-1}, using S_8 angular quadrature, with 3 uniform spatial cells. The left boundary condition is an isotropic incident flux, normalized to yield a unit current; the right boundary condition is a vacuum boundary. The

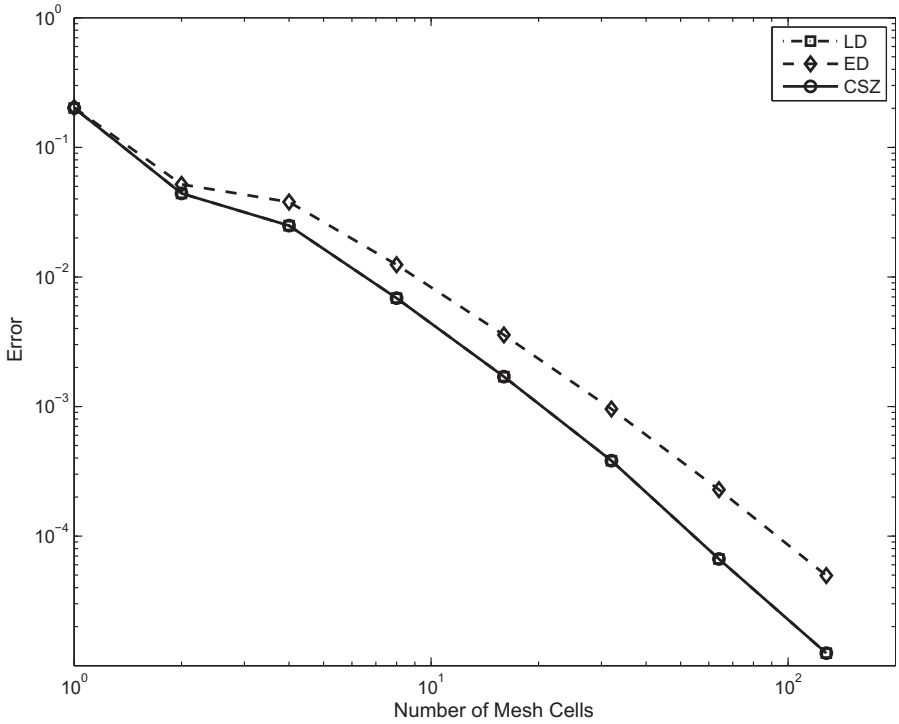

Fig. 10. Rate of convergence for a slab with a distributed inhomogeneous volumetric source and c = 0.9.

Table 1
Number of matrix inversions required for the ED and CSZ methods relative to LD for the case of a pure absorber slab.

Number of Cells	Method	
	ED	CSZ
1	5.63	6.63
2	5.50	3.31
4	5.63	1.91
8	7.78	1.14
16	5.00	1.06
32	4.76	1.00

average scalar flux for a given cell is plotted at the midpoint of the cell. The convergence rate plot for LD and CSZ is given in Fig. 8. Fig. 8 shows that CSZ is more accurate than LD on coarse meshes and that as the mesh is refined, CSZ becomes equivalent to LD.

Table 2
Number of matrix inversions required for the ED and CSZ relative to LD for isotropic flux incident on a slab with $c = 0.5$.

Number of Cells	Method	
	ED	CSZ
1	10.93	11.36
2	14.03	4.94
4	11.47	4.44
8	13.14	1.32
16	11.12	1.02
32	10.89	1.01

Table 3
Number of matrix inversions required for the ED and CSZ methods relative to LD for a slab with a distributed inhomogeneous source and $c = 0.9$.

Number of Cells	Method	
	ED	CSZ
1	6.21	1.00
2	6.45	1.00
4	6.39	1.00
8	9.55	1.00
16	6.58	1.00
32	6.32	1.04

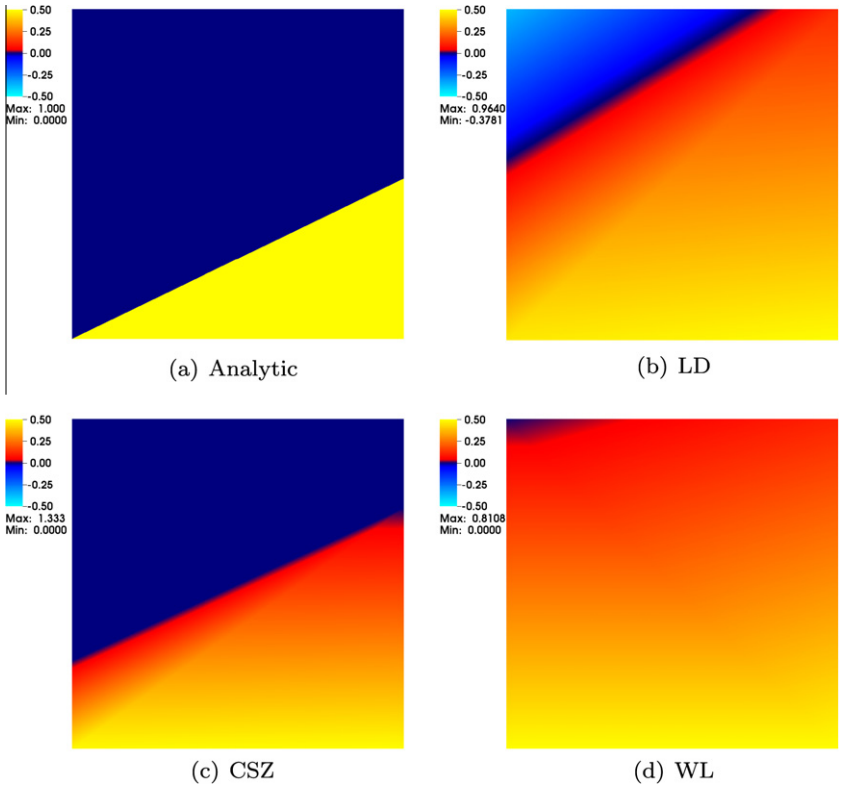

Fig. 11. Comparison of the $\widetilde{\psi}(s,t)$ calculated with each numerical method versus the analytic solution, $\psi(s,t)$, for grazing incident flux into a single voided cell.

5.1.3. Isotropic incident flux on a slab with scattering

We again consider a 12 cm wide slab with, isotropic, left incident, unit current angular flux, vacuum boundary conditions on the right face, no distributed source, an S_8 angular quadrature, but with a scattering material: $\sigma_t = 1$ cm^{-1}, and the scattering ratio $c = \sigma_s/\sigma_t = 0.5$. Fig. 9 shows that ED is more accurate than both LD and CSZ. However, Fig. 9 also shows that LD, CSZ, and ED all have the same order of accuracy as the mesh is refined. ED is more accurate than LD and CSZ. However, this is a problem-dependent phenomena as shown by the final slab problem.

5.1.4. Homogeneous volumetric source in a slab with scattering

The last slab test problem is similar to the first two problems, but with vacuum boundary conditions on both faces, an isotropic unit source distributed throughout the slab, $\sigma_t = 1$ cm^{-1}, and $c = 0.9$. It should be noted that CSZ is in fact plotted in Fig. 10, but in this problem LD does not produce any significant negativities, so LD and CSZ produce essentially identical results. By comparing Fig. 9 and Fig. 10 it is clear, that as a problem becomes less and less like a pure absorber, and the angular flux solution, ψ, transitions from having positive curvature to having negative curvature, ED becomes less accurate than both LD and CSZ due to the inherently positive curvature of the ED scheme.

5.1.5. Slab computational costs

The computational costs for the three slab test problems are listed in Table 1, Table 2, and Table 3. Overall, the data from these tables indicates that CSZ is generally less costly than ED, and in many instances, CSZ does not even require the solution of a nonlinear system of equations because the initial LD guess is sufficient. Since ED yields the exact analytic solution for a pure absorber, its convergence data was omitted from Fig. 8, but its cost is presented in Table 1 to illustrate the significant cost inherent to ED, even though $\widetilde{\psi}_{ED}$ is the exact solution for a pure absorber. The other significant trend which must be highlighted is the decrease in computational cost CSZ benefits from as the mesh is refined. This trend is again a direct result of CSZ initially assuming the LD solution, coupled with the fact that LD yields an everywhere non-negative solution with mesh refinement. The exception to this trend comes in the volumetric source problem. In the source problem, as the mesh is refined, LD begins to generate negative values of $\widetilde{\psi}_{LD}$ at the *inflow* of boundary cells for directions with $|\mu_d| \approx 0$. This is a result of the LD solution generating values of $\psi_{X,i,d}/\psi_{A,i,d} > 1$. The negativities are on the order of 10^{-4}, which is quite small, but they cause CSZ to transition to a nonlinear solution.

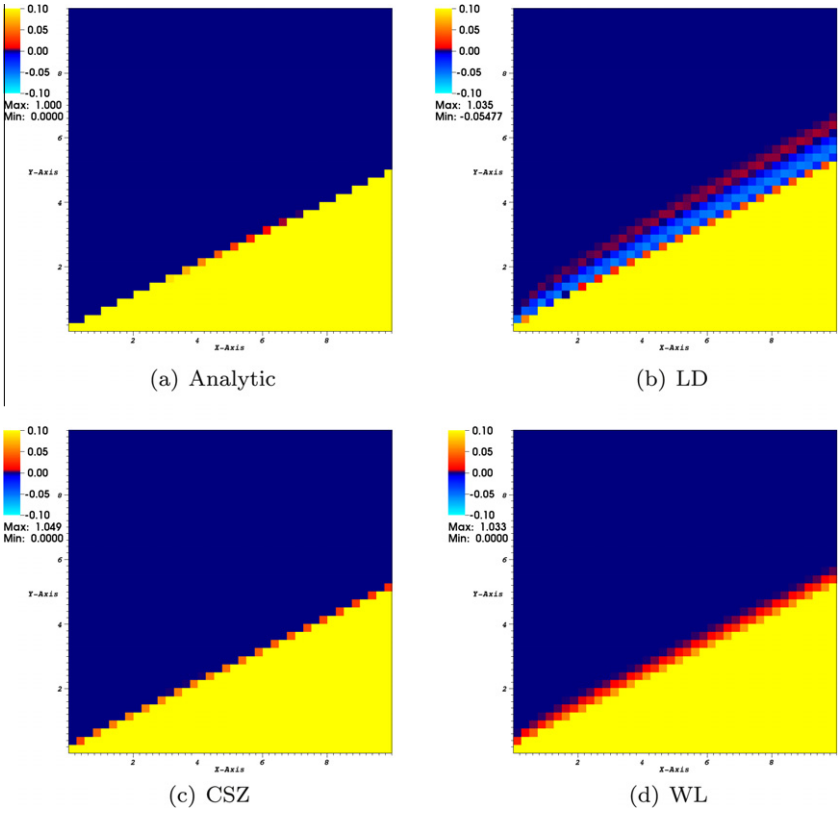

Fig. 12. Plots of $\psi_{A,i,j,d}$ for the discretized void problem with grazing incident flux with $\Delta x_i = \Delta y_j = 0.2$cm. Plots use a linear scale to illustrate negativities and oscillations of LD.

5.2. Rectangular computational results

In slab geometry, LD produces negative angular flux solutions only in optically thick cells. However, in rectangular geometry, negativities can occur anywhere the solution is rapidly varying, including voids. We therefore present a series of test problems which are known to produce poor results when using the LD spatial discretization in 2-D.

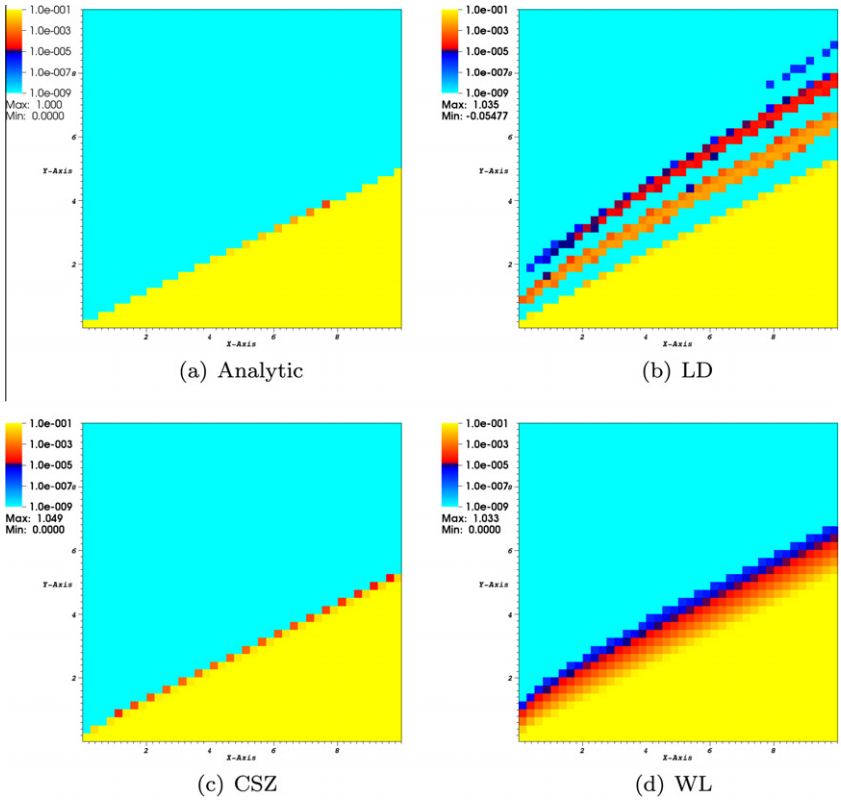

Fig. 13. Plots of $\psi_{A,i,j,d}$ for the discretized void problem with grazing incident flux with $\Delta x_i = \Delta y_j = 0.2$ cm. Plots use a logarithmic scale to highlight WL numerical diffusion. Negativities and 0s are represented as the minimum of the color scale.

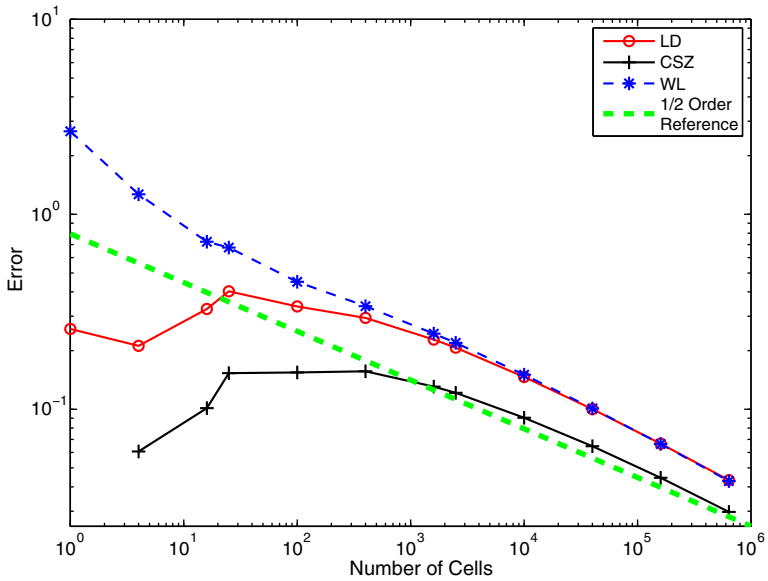

Fig. 14. L2 norm order of convergence plot for the discretized void problem.

5.2.1. Grazing incident flux in a single voided cell

The first test problem is a single cell test case that illustrates the negativities that can occur in voids with glancing incidence angular flux. We choose a 1 cm $\times$ 1 cm void cell with a beam of radiation incident along the bottom face in the direction $\mu_d = 0.90$ and $\eta_d = \sqrt{1-\mu_d^2}$. The incident angular flux has a value of 1 particles/cm^2 s sr. Fig. 11 shows the calculated angular flux solution $\widetilde{\psi}$ on the interior of the cell for each method versus the exact analytical solution. LD clearly propagates a significant negative outflow along the top face of the cell, while the CSZ and WL schemes produce strictly non-negative outflows. Of greater interest is the comparison of $\widetilde{\psi}_{CSZ}$ and $\widetilde{\psi}_{WL}$. By not satisfying Eq. (20b) and Eq. (20c), WL significantly

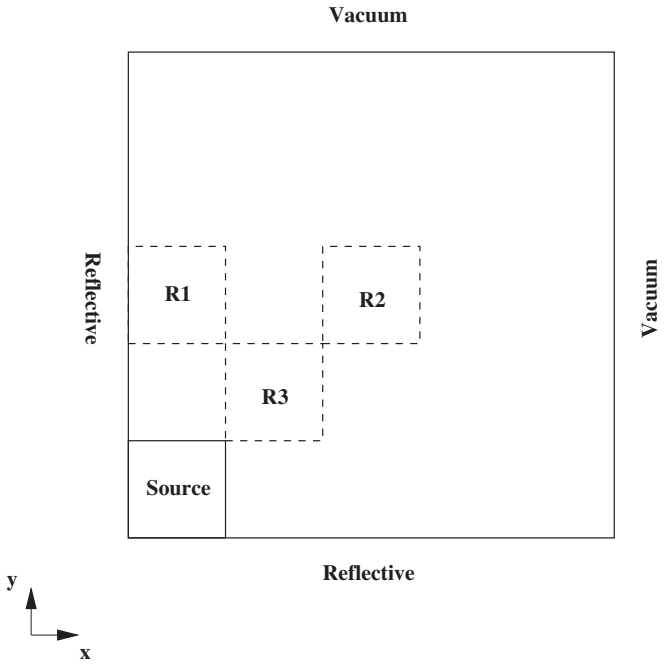

Fig. 15. Diagram of the iron-water like rectangular geometry test problem, and location of the three regions, *R*1, *R*2, and *R*3, for which the total reaction rates were recorded.

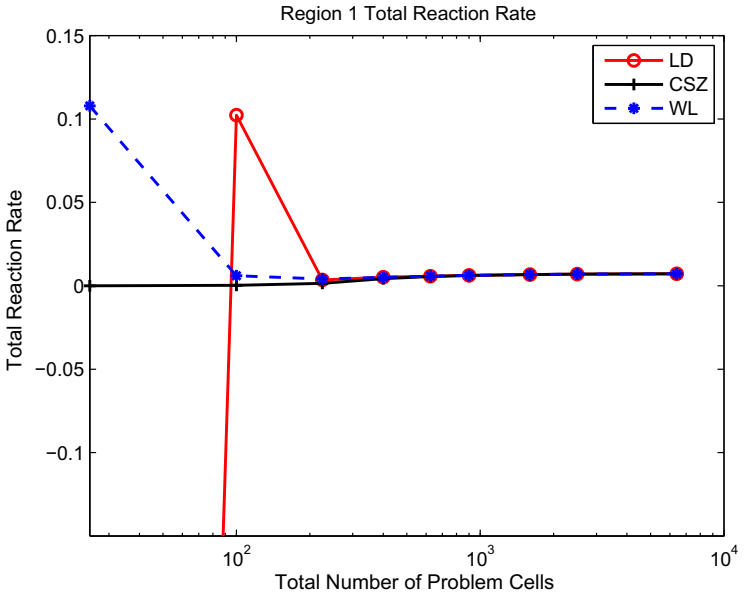

Fig. 16. Total reaction rates for each method in *R*1 of the iron-water like problem.

increases numerical diffusion within the cell. The implications of this increased numerical diffusion are not obvious with a single cell test case, but our next problem clearly illustrates the degrading effect on global solution accuracy for larger problems.

5.2.2. Grazing incident flux in a discretized voided domain

Our second rectangular geometry test problem consists of a 10 cm × 10 cm void, divided into uniform cells, $\Delta x_i = \Delta y_j$. A beam of radiation is incident along the bottom face of the first (left-bottom) cell in the direction $\mu_d = 0.90$, $\eta_d = \sqrt{1-\mu_d^2}$, with vacuum boundary conditions along all other faces. The incident angular flux has a value of 1 particles/cm^2 s sr. Fig. 12 shows a linear plot of the reference and the numerically calculated values of $\psi_{A,i,j,d}$ when the problem is divided into 1600 total mesh cells. From Fig. 12, it is clear the LD solution is exhibiting two important, non-physical qualities:

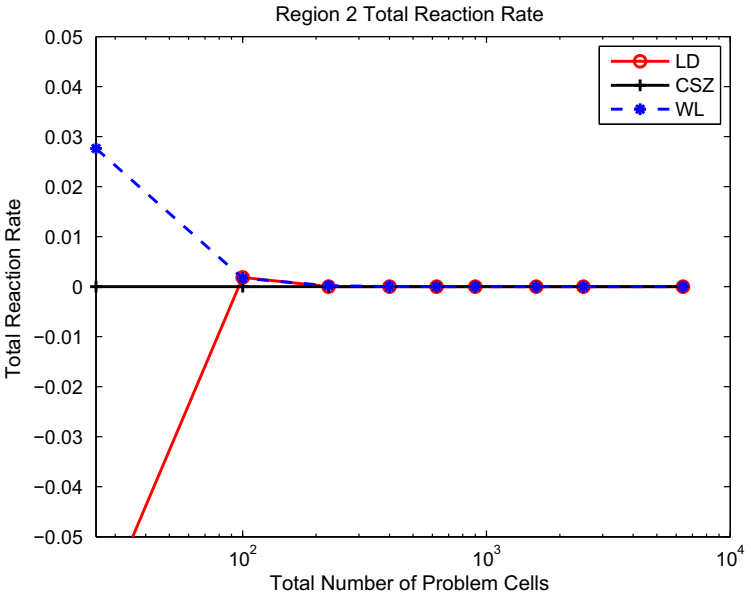

Fig. 17. Total reaction rates for each method in $R2$ of the iron-water like problem.

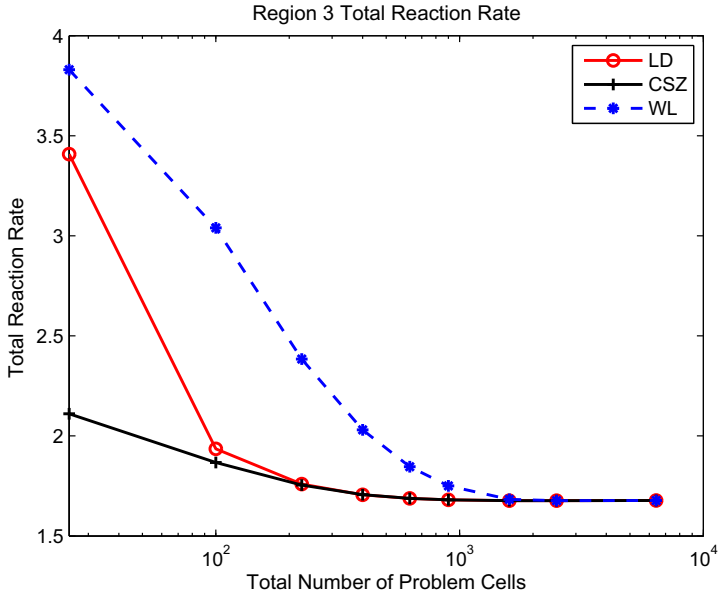

Fig. 18. Total reaction rates for each method in $R3$ of the iron-water like problem.

1. negativities,
2. oscillations and angular flux propagation into the region where $\psi_{ex}(x,y) = 0$.

Though WL produces a strictly non-negative angular flux solution without any oscillations, numerical diffusion seriously degrades the solution. This is apparent from the linear graph, Fig. 12, but Fig. 13 is provided to make this more apparent. CSZ largely avoids any numerical diffusion; the strictly non-negative piecewise linear flux shape strongly inhibits the numerical spreading of the angular flux solution into the region where $\psi(x,y) = 0$. Looking beyond this single refinement, the L_2 norm of the error is plotted in Fig. 14. Two trends are demonstrated by Fig. 14:

1. for this problem, CSZ is always more accurate than LD and WL and
2. all three numerical methods approach order 1/2 convergence, which is the theoretically-predicted value for linear transport problems with singularities [23].

It should be noted that CSZ yields the exact value for $\psi_{A,i,j,d}$ with a single cell, resulting in a zero error which cannot be plotted on a logarithmic scale graph. This result is expected because the solution to this problem can be exactly represented in a single cell by the trial space, and the moment specification of the inflow flux uniquely defines that flux distribution. However, when the problem spans more than one cell, the moment specification of the inflow flux uniquely defines that flux distribution only for the first cell. Thus the solution remains exact only in that cell.

Table 4
Number of matrix inversions relative to LD for a grazing incident flux on a discretized voided domain.

Number of Cells	Method	
	CSZ	WL
1	8	2
4	4.75	1.75
16	2.69	1.75
25	2.80	1.76
100	1.99	1.74
400	3.07	3.15
1.6K	1.28	1.32
2.5K	1.23	1.26
10K	1.11	1.13
40K	1.05	1.07
160K	1.03	1.03
640K	1.01	1.02

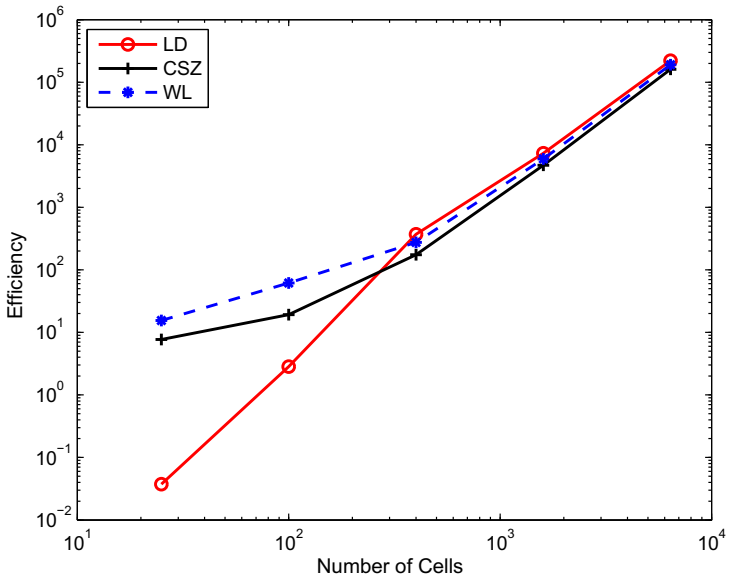

Fig. 19. Relative computational efficiency of each method for R1 of the iron-water like problem.

The dashed green line in Fig. 14 is provided as a reference line of order 1/2 convergence rate.

5.2.3. Variations on the standard iron-water problem

Our final problem is similar to the classic iron-water problem. As shown in Fig. 15, the test problem consists of a 50cm x 50cm, homogeneous rectangle, with $\sigma_t = 1.0\,\text{cm}^{-1}$, a scattering ratio of $c = 0.75$, and an isotropic source in the lower left 10cm x 10cm corner of the problem, with an average source strength of $1/4\pi$ particles/cm^3 s sr. The bottom and left boundaries are reflective, while the top and right boundaries are vacuum. The problem was discretized with a uniform spatial discretization, $\Delta x_i = \Delta y_j$, with a total mesh size varying between 25-6400 cells, using a level-symmetric S_8 angular quadrature. The total reaction rate was calculated within three square regions, denoted $R1$, $R2$, and $R3$ respectively, as shown in Fig. 15. Plots of the reaction rate within each each region of interest are given in Figs. 16–18. The figures indicate several important trends:

1. WL and CSZ are always non-negative,
2. WL and CSZ converge to the LD solution,
3. LD can calculate significant negativities,
4. LD is subject to oscillations,
5. CSZ coarse mesh calculations are significantly more accurate than LD and WL solutions on the same mesh, and
6. WL can be significantly less accurate than LD (see Fig. 18).

5.2.4. Rectangular computational costs

The benefits of WL, requiring at most 2 matrix inversions to provide a strictly non-negative angular flux solution, is obvious when considering the first entry of Table 4. In the single cell void problem, there is only 1 cell with 1 direction that requires a strictly non-negative modification. As expected, WL requires two times more work than LD. CSZ requires multiple Newton iterations, and thus does about eight times more work than LD. However, Table 4 also clearly illustrates the computational costs associated with the numerical diffusion of WL. If CSZ and WL were applied in the same number of cells in the large void problems, we might expect to maintain the single cell ratio of four times more computational work for CSZ than WL. However, this is obviously not the case. By numerically diffusing the incident angular flux in the WL scheme, many more cells require a modification of the LD solution to eliminate the negativities associated with $\widetilde{\psi}_{LD}$, and thus the amount of work required for the WL scheme increases.

Efficiencies of each method for calculating the scalar flux within the 3 regions considered are plotted in Fig. 19 for R1, Fig. 20 for R2, and Fig. 21 for R3. The efficiency plots highlight several features of the CSZ scheme:

1. CSZ is always more efficient than LD at coarse mesh refinements,
2. CSZ can be orders of magnitude more efficient than LD and WL with coarse meshes, and
3. In the fine mesh limit, CSZ is never more than 30% less efficient than LD or WL.

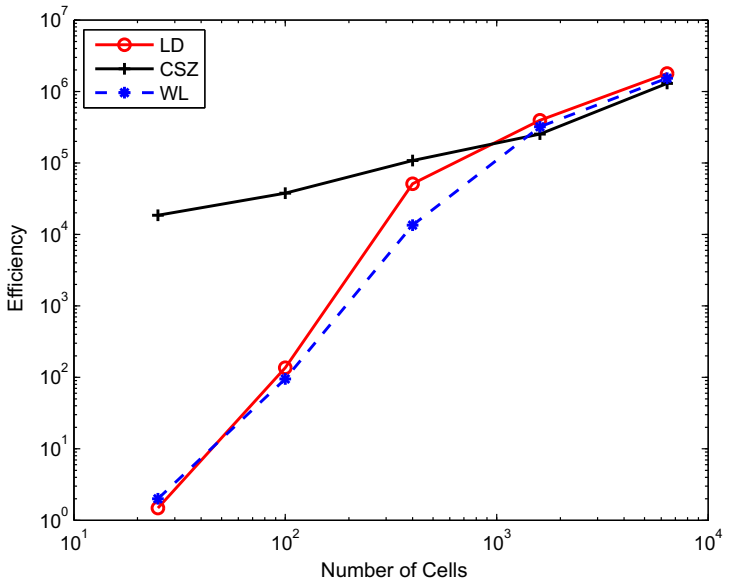

Fig. 20. Relative computational efficiency of each method for R2 of the iron-water like problem.

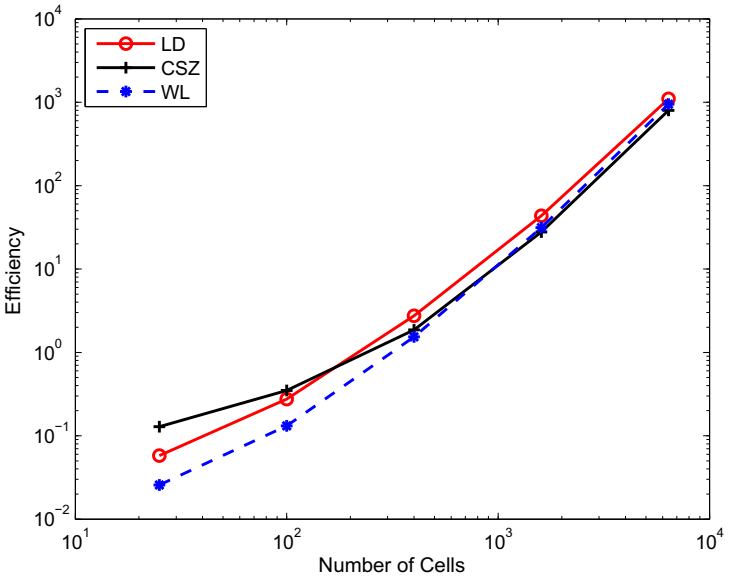

Fig. 21. Relative computational efficiency of each method for R3 of the iron-water like problem.

6. Conclusions

CSZ is always as accurate or more accurate than LD. The performance of CSZ relative to ED and WL is problem-dependent. However, the performance of ED and WL relative to LD is problem-dependent. In the problems we considered, the computational cost of using the CSZ method never significantly exceeded that of the ED method, and in most cases the computational cost of the CSZ method was significantly less than that of ED. This is due to the fact that ED always requires the solution of a nonlinear system of equations, whereas by initially assuming the LD solution, CSZ does not always require a nonlinear solve. For problems with a small number of spatial cells, CSZ is significantly more computationally expensive than the WL ad-hoc fixup. However, for larger more realistic problems, the increased computational cost of CSZ relative to WL quickly vanishes, and in some cases, applying the CSZ scheme becomes less expensive than WL. This result stems from the increased numerical diffusion associated with the ad-hoc WL fix-up. Because all the spatial moment equations are not satisfied, the angular flux is smeared into additional spatial cells, requiring additional application of the ad-hoc fix-up, resulting in increased computational work. On coarse meshes, CSZ can be orders of magnitude more computationally efficient than LD or WL. In the fine mesh limit, CSZ is at most 30 percent less computationally efficient than LD or WL.

CSZ is envisioned as a supplement to the ubiquitous LD discretization for those applications that require strictly nonnegative solutions. The CSZ scheme has been presented here for slabs and rectangular geometries, but is easily extensible to 3-D orthogonal (brick) meshes as well as non-orthogonal 2-D and 3-D geometries. In addition, work is ongoing to investigate more advanced solution techniques for the scheme as well as its behavior in highly diffusive problems. Source iteration is inadequate for such problems, so we are investigating a Jacobian-free Newton–Krylov method with DSA preconditioning. Radiative transfer in the high energy density regime is one of the most obvious applications for the CSZ method. This regime often includes both optically-thin and highly diffusive regions. Both advanced solution techniques and good behavior in the thick diffusion limit are required for radiative transfer calculations. Like the LD method, the CSZ method can be expected to preserve the thick diffusion limit in 2-D only on triangles and in 3-D only on tetrahedra [24].

References

[1] E.W. Larsen, R.E. Alcouffe. The linear characteristic method for spatially discretizing the discrete-ordinates equations in (x,y)-geometry. ANS/ENS Joint Topical Meeting, Mathematical Methods in Nuclear Engineering, Munich, FRG, April, 1981.
[2] Edward W. Larsen, On numerical solutions of transport problems in the diffusion limit, Nuclear Science and Engineering 83 (1983) 90–99.
[3] Edward W. Larsen, J.E. Morel, Warren F. Miller Jr., Asymptotic solutions of numerical transport problems in optically thick, diffusive regimes, Journal of Computational Physics 69 (1987) 283–324.
[4] M.L. Adams, T.A. Wareing, W.F. Walters, Characteristic methods in thick diffusive problems, Nuclear Science and Engineering 130 (1988) 18–46.
[5] E.E. Lewis, W.F. Miller, Computational Methods of Neutron Transport, American Nuclear Society, La Grange Park, IL, 1993.
[6] Kirk Mathews, Glenn Sjoden, Bryan Minor, Exponential characteristic spatial quadrature for discrete ordinates radiation transport in slab geometry, Nuclear Science and Engineering 118 (1994) 24–37.
[7] Bryan Minor, Kirk Mathews, Exponential characteristic spatial quadrature for discrete ordinates radiation transport with rectangular cells, Nuclear Science and Engineering 120 (1995) 165–186.
[8] Wallace F. Walters, Todd Wareing, An accurate, strictly-positive, nonlinear characteristic scheme for the discrete-ordinate equations, Transport Theory and Statistical Physics 25 (1996) 197–215.
[9] Marvin L. Adams, Edward W. Larsen, Fast iterative methods for discrete-ordinates particle transport calculations, Progress in Nuclear Energy 40 (2002) 3–159.

[10] R.E. Alcouffe, E.W. Larsen, W.F. Miller, B.R. Wienke, Computational efficiency of numerical methods for the multigroup, discrete-ordinates neutron transport equation: the slab geometry case, Nuclear Science and Engineering 71 (1979) 111–127.
[11] Todd A. Wareing, An exponential discontinuous scheme for discrete-ordinate calculations in Cartesian geometries, in: Joint International Conference on Mathematical Methods and Supercomputing for Nuclear Applications, Saratoga Springs, N.Y., Oct. 5–9, 1997.
[12] R.E. Alcouffe, A robust linear discontinuous method for the RZ, S_n transport equation, Transactions of the American Nuclear Society 89 (2003) 363.
[13] Erin D. Fichtl, James S. Warsa, Jeffery D. Densmore, The Newton–Krylov method applied to negative-flux fixup in S_n transport calculations, Nuclear Science and Engineering 165 (2010) 331–341.
[14] Peter Maginot, Jim Morel, Jean Ragusa, A positive non-linear closure for the S_n equations with linear discontinuous differencing, in: Proceedings of the International Conference on Mathematics, Computational Methods, and Reactor Physics (M&C 2009), Saratoga Springs, N.Y., May 3–7, 2009.
[15] Kirk A. Mathews, Adaptive characteristic spatial quadratures for discrete ordinates neutral particle transport – the slab geometry case, Transport Theory and Statistical Physics 19 (6) (1990) 419–458.
[16] Kirk A. Mathews, Bryan M. Minor, Adaptive characteristic spatial quadratures for discrete ordinates neutral particle transport- the rectangular cell case, Transport Theory and Statistical Physics 22 (5) (1993) 655–685.
[17] T.A. Wareing, W.F. Walters, J.E. Morel, A diffusion-accelerated solution method for the non-linear characteristic scheme, in: Proceedings of the International Conference on Mathematics and Computations, Reactor Physics, and Environmental Analyses, April 30–May 4, 1995, Jantzen Beach Red Lion Hotel, Portland Oregon, vol. 2, pp.1335–1341, 1995.
[18] R. Vichnevetson, Computer Methods for Partial Differential Equations, Volume 1, Elliptic Equations and the Finite-Element Method, Prentice Hall, Inc., New Brunswick, NJ, 1981.
[19] MATLAB. The MathWorks, Natick, MA, 2007.
[20] S. Hamilton, M. Benzi, J. Warsa, Negative flux fixups in discontinuous finite element SN transport, in: Proceedings of the International Conference on Mathematics, Computational Methods, and Reactor Physics (M&C 2009), Saratoga Springs, New York, 2009.
[21] J. Nocedal, Stephen J. Wright, Numerical Optimization, Springer Science + Business Media, LLC., New York, NY, 2000.
[22] James S. Warsa, Analytical S_n solutions in heterogeneous slabs using symbolic algebra computer programs, Annals of Nuclear Energy 29 (2002) 851–874.
[23] Claes Johnson, Juhani Pitkaranta, Convergence of a fully discrete scheme for two-dimensional neutron transport, SIAM Journal on Numerical Analysis 20 (5) (1983) 951–966.
[24] Marvin L. Adams, Discontinuous finite element transport solutions in thick diffusive problems, Nuclear Science and Engineering 137 (2001) 298–333.